Chiral Liquid Crystalline Properties of Cellulose Nanocrystals: Fundamentals and Applications

Aref Abbasi Moud*

ACCESS | Metrics & More | Article Recommendations

ABSTRACT: By using an independent self-assembly process that is occasionally controlled by evaporation, cellulose nanocrystals (CNCs) may create films (pure or in conjunction with other materials) that have iridescent structural colors. The self-forming chiral nematic structures and environmental safety of a new class of photonic liquid crystals (LCs), referred to as CNCs and CNC-embedded materials, make them simple to make and treat. The structure of the matrix interacts with light to give structural coloring, as opposed to other dye pigments, which interact with light by adsorption and reflection. Understanding how CNC self-assembly constructs structures is vital in several fields, including physics, science, and engineering. To constructure this review, the colloidal characteristics of CNC particles and their behavior during the formation of liquid crystals and gelling were studied. Then, some of the recognized applications for these naturally occurring nanoparticles were summarized. Different factors were considered, including the CNC aspect ratio, surface chemistry, concentration, the amount of time needed to produce an anisotropic phase, and the addition of additional substances to the suspension medium. The effects of alignment and the drying process conditions on structural changes are also covered. The focus of this study however is on the optical properties of the films as well as the impact of the aforementioned factors on the final transparency, iridescent colors, and versus the overall response of these bioinspired photonic materials. Control of the examined factors was found to be necessary to produce reliable materials for optoelectronics, intelligent inks and papers, transparent flexible support for electronics, and decorative coatings and films.
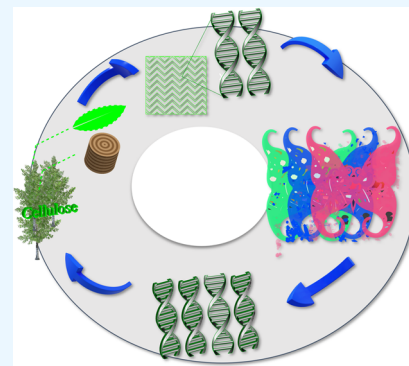
1. INTRODUCTION

A covalent acetal oxygen link forms between the C1 of one glucose ring and the C4 of the next to form cellulose, which is made up of a linear chain of glucose molecules, resulting in an elementary fibril that can be connected to form microfibrils with a width of 5−50 nm and a span of a few micrometers, with crystalline or amorphous areas.[1] While fibrillation can create cellulose nanofibrils (CNFs), acid hydrolysis can yield cellulose nanocrystals (CNCs) from wood (a technique that eliminates amorphous areas). The length and diameter of CNCs have been measured to be 100−300 nm and 3−10 nm, respectively; however, this varies depending on the source of the CNC and the method of development.

A family of materials known as "liquid crystals" (LCs) display forms of matter which are neither crystalline materials nor isotropic liquids when specific conditions are satisfied (such as temperature, pressure, and concentration). Depending on how a solid transitions through mesophases to become an isotropic liquid, LCs are categorized as "lyotropic" or "thermotropic". The growth of large-scale structures from submicron unit characteristics in the chiral self-assembly of nanoconstruction blocks can result from liquid crystal phase transformation. This phase transition offers a technique for creating useful materials with specialized physical, electrical, and optical properties.[2] Amyloid

fibrils[3] and deoxyribonucleic acid (DNA) filaments[4] are two examples of colloidal self-organizing systems that exhibit unique chirality by their bending arrangement of building parts.

In both real-world systems and model colloidal self-assembling particles like rod-like viruses,[5] transferring chirality over length scales (e.g., nm, μm) is difficult. The single-handedness of many key bios-found molecules, homochirality, is ubiquitous and a key signature of life on our planet. All living organisms use L-amino acid and D-sugar almost exclusively as building blocks for proteins and nucleic acids.[6] Geometrically speaking, an item is chiral if it cannot be accurately translated or rotated to produce its mirror counterpart. At almost every length scale, chirality has been seen phenomenologically; for instance, the spin and motion direction of a massless subatomic particle define its chirality. Interesting instances of macroscopic chirality include the tendrils of plants,[7] the right- and left-handed (dextral

and sinistral) shells of snails,[8] where a single gene expression influences snail reproduction, and the astonishing expansion of solely left-handed long tusks in narwhals.[9]

In a colloidal suspension, bioderived nanoparticles called CNCs self-assemble to form a left-handed chiral nematic (cholesteric) phase.[10] While chiral scaffolding and long-lasting photonic colorants have been produced using their propensity for self-assembly, the origin of their mesophase chirality is still a hotly debated topic.[10,11] CNCs twist because of the chemical chirality of the α-1,4-D-glucose repeating unit, although it is not known how (or whether) this little twist that later causes a twist in individual CNCs is sufficient to generate chirality in the mesophase. Furthermore, chirality attribution is challenging due to the CNC population's extremely polydisperse particle size and shape.[12]

Owing to its chiral spiral geometry, the CNC LC film seems to have a vibrant structural color, but internal structures also create circularly polarized reflection, giving it extraordinary optical properties. This regular nanostructure has inspired and benefited prior studies that have studied and analyzed several CNC-based photonic crystal material components.[13,14] Until recently, no thorough analysis of CNC-produced photonic functional materials has been done. This review seeks to examine CNC liquid crystal formation fundamentals and some of its very recent applications. Investigated first are the basics of architectural colors, photonic crystals, and liquid crystal states. The fabrication of CNC-based color materials, as well as their optical characteristics and regulatory processes, will be discussed after that. This served as the foundation for a summary of the application research for CNC-based chiral nematic liquid crystal films in many sectors. Investigating the adaptability of structural color materials with CNC bases is another emphasis.

2. BACKGROUND

2.1. Structural Color. Nature has created a wide range of substances and arranged them in such a way that their coloring shines out. Most of the coloring in living things comes from structure colors or pigment colors. Contrarily, structural colors result from organized geometrical (photonic crystal) structures that may precisely regulate the dispersion and reflection of light on a surface or the skin. It is common knowledge that when light impinges on a substance's surface light scattering, diffraction, and diffuse scattering take place in the substance's interior structure. During this time, the lights will once again be visible to humans, and the many colors will be audible.

As a result, the color that is seen depends on the internal structure, and if the substance's microstructure and composition do not change, the color will also not change. Structured colors are more ecologically sound than pigments colors because they never fade, and they pose no toxicity. The two primary categories of structural colors are angle-dependent architecture colors and angle-independent structure colors. (i) For angle-dependent structural colors, depending on the angle of view, the structure has a regular inner structure in the material that shows various colors. Natural species with this type of structural color include butterfly wings,[15] beetles,[16] and opals.[17] (ii) Angle-independent structural colors (angle-independent structural colors) generate color due to light dispersion within the short-range ordered nanostructure, and the array lacks periodicity and displays structural colors that are angle independent at longer spatial scales.

The angle-dependent structural colors that are the focus of this review can be found in the scales of the spotted parachute

bird, blue-skinned mandrill,[18] Morpho butterfly wings,[19] and long-horned beetle[20] in addition to examples provided earlier. Although structural colors have outstanding optical properties, full control over the photon transmission channel in conventional structural materials is limited, which can have a substantial impact on the development of these materials as well as their usage in photonic devices and electronic circuits. In terms of applications, photonic integrated circuits are most used in fiber-optic transmission, but they can also be found in biomedical and photonic computer applications. As a result, the structural color's superiority in practical applications cannot be highlighted enough due to ease of processing and evidence of its widespread adoption. Color changes in these structure are also tunable, and according to principles, structural color materials change color in response to humidity,[21] temperature,[22] pH,[23] dielectric property of solvent,[24] presence of dopants,[25] electrical and magnetic signals,[26] enzymes,[27] alcohol,[28] urea, and heavy metals.[29] Structural color material can be used to color encrypt[30] a structure in a wide range of optical fields, not just responsive optical devices.

3. PHOTONIC CRYSTAL

More researchers are upgrading the color-creation method as nanotechnology advances. Structural color is made by the photonic crystal structure inside the item; therefore, the color is produced because of light interaction with the structure. On the basis of uncontrolled atom emissions and photon localization, John and Yablonovitch[31] introduced the idea of photonic crystals in 1987. From a physics perspective, an organized arrangement of nanostructures with various refractive indices in space results in the formation of a photonic crystal. Recurrent variations in the index of refraction of space would control photon transmission in a manner analogous to that for the semiconductor lattice with the electric wave function; therefore, terminologies used in these two branches of science are very similar. As the electromagnetic wave passes through the photonic crystal, Bragg scattering alters it, creating an energy band structure like that of a semiconductor. A photon energy band is the name for this kind of energy band. When the disparities in refractive indices between various materials reach a critical level, electromagnetic waves with precisely matched wavelengths between photonic energy bands are prevented from passing through the crystal. The photonic bandgap is the name given to this frequency range. Optics researchers are interested in the peculiar optical features of photonic crystalline forms, such as slow light effect and negative refraction.[32]

Natural selection is the process through which many of the useful structures of living things developed contribute to passing genes and the allure of these animals/plants. One of the forms in biological systems that has drawn the attention of scientists from many fields is chiral photonic crystals. Since these natural patterns are produced using a range of elements, it is essential to comprehend the systematic organization in nature, with the aim of copying inspired structures within an arsenal of manmade objects such as CNCs. Nanostructures, such as those seen in beetle shells, butterfly wings, and peacock feathers, can display color without use of pigment or dyes. For instance, the iridescent *Plusiotis bacardi* (outer shell) of the beetle has a novel microstructure that may regulate the polarization and wavelength of reflected light.[33]

Scientists are trying to replicate these templates and create the material with certain qualities that are inspired by the structure of nature. However, the growth of artificial crystalline materials

is still slow due to a lack of accurate photonic structural systems and efficient fabrication procedures. On the other hand, scientists started employing quick and efficient methods to search for novel materials in nature. The evolution of CNCs into a 1D chiral nanorod with excellent mechanical, photonic, and electromechanical characteristics has been facilitated by the development of characterization technologies. By adjusting the chiral nematic nanostructures, material scientists showed how to colorize CNC-based films, revealing a 1D photonic crystal feature.

The pitch size of LCs is one of its distinguishing characteristics. Helices are without a doubt among the most beautiful chiral structures. A helix is described by its periodicity (pitch, p) or wavenumber $q = \frac{2\pi}{p}$, as well as its handedness, which is defined as positive for a right-handed or clockwise twist and negative for a left-handed or counterclockwise twist. The chirality concept for molecules can be extended to particles as well; all cellulose fibrils and crystals with detectable chirality are right-handed (making left-handed chiral structures), according to magnified microscope images.[10] Schematic pitch and chiral structures of CNCs are shown in Figure 1.
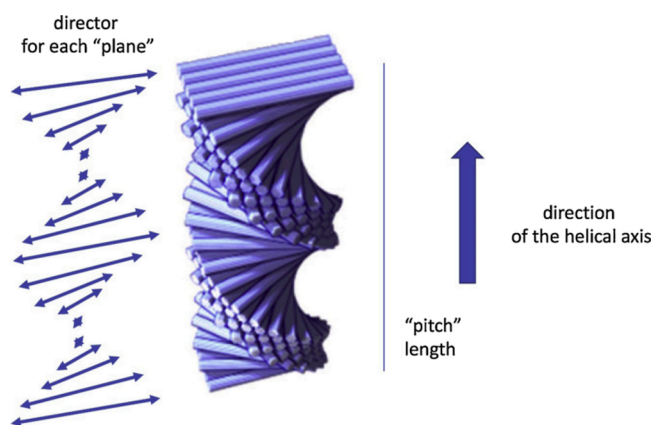

Figure 1. Ordering of the CNC dispersions is chiral nematic depending on solution temperature, concentration, and properties of CNCs. The length of the "pitch" is equivalent to a full director turn. Schematic displaying the structure also known as "Bouligand structure". Copyright 2019 Springer Nature. Adapted with permission from ref 34.

3.1. Liquid Crystalline State Definitions. According to Onsager's model,[35] the volume fraction required for the production of liquid crystals is inversely related to the rod aspect ratio; therefore, if CNCs are manufactured to be longer and thinner, the initial concentration required to see the liquid crystal crossover should drop. Bacterial cellulose dispersion, which has an aspect ratio of 50 to 100 and lengths ranging from 1 to 2 μm, exhibits nematic organization much sooner than CNCs; CNF particles ought to behave similarly. However, the aspect ratio cannot be raised indefinitely to move the transition points to lower volume fractions. The fact that the volume fraction for showing glassy behavior and the liquid crystalline transition are so close together makes passing the liquid crystalline transition point one disadvantage of increasing the aspect ratio. When liquid crystal transitions from bacterial cellulose > cellulose nanofibrils > cellulose nanocrystals, a glassy state is seen due to the longer and more wavy molecules. Reaching glassiness gives kinetically arrested particles the tendency to generate chiral structures. Besides the aspect ratio, generated by the overlap of

electrical double layers, electrostatic repulsive forces and attraction van der Waals forces interact with colloids and can move transition boundaries, i.e., the point of transition from isotropic to liquid crystalline and to fully liquid crystalline transition points.

Moreover, the flexibility (persistence length) of rods can also affect transition points. It is defined as $\frac{L}{l_p}$, in which l_p is the persistence length, a quantity that can be determined from static light scattering or direct visualization measurements and can also be used to describe flexibility. The persistence length is the distance along a rod's contour at which two spots' ensemble-averaged mutual orientation becomes decorrelated for the first time. Thus, $\frac{L}{l_p} \ll 1$ for stiff rods and $\frac{L}{l_p} \approx 1$ for semiflexible filaments. Low aspect ratio particles, predominantly inorganic materials like boehmite and hematite, are hard, whereas nanotubes and cellulose fibers are more flexible due to their length. Single-wall carbon nanotubes, for example, have been found to have a persistence length of 30–170 μm,[36] which is likewise diameter dependent.[37] The rheology of biopolymer actin at higher frequencies reveals a semiflexible nature.[38] At higher frequencies, the rheological response is a function of bending modulus or stiffness, which is a function of persistence length.[39]

Concentration is yet another factor in changing transition points. As the particle concentration increases, the system approaches a glassy state or transitions from an isotropic to a nematic or higher-order liquid crystalline form. Carbon nanotubes reportedly experienced the same transformation from an isotropic to a glassy state while displaying no liquid crystal states, according to previous research.[40] The glassy state is initiated prior to the creation of liquid crystals due to the high polydispersity and aspect ratio of carbon nanotubes (CNTs). Higher quantities of carbon nanotubes are difficult to analyze due to the difficulty in preventing particle aggregation. Glass transition has only been noticed for highly dispersed carbon nanotubes at low threshold concentrations, and the only nematic ordering (no chirality) of carbon nanotubes has been characterized as a liquid crystal phase thus far. It is difficult to see higher-order liquid crystal phases utilizing carbon nanotubes because of the significant size variation of the tube length.

According to the authors in ref 41, polydispersity caused by end-to-end agglomeration or fragmenting of the virus as well as the existence of any impurity in solution are especially sensitive to the existence of a crystalline form in the tobacco virus. Since the population of the *fd* virus can be made to have a polydispersity of 1, it can be used as a model system to see the effect of parameters such as ionic strength on its transition points. In fact, Kang and Dhont[42] recently found that viral suspension studies at low salt limits clearly showed a change from cholesteric (also known as chiral nematic) to the glassy state. When viral concertation is more than 12 mg/mL, the cholesteric phase is locked because the nonequilibrium texture created by shearing in the cholesteric phase no longer relaxes but instead vitrifies in a glassy state. Strong repulsive forces from nearby charged particles confine the *fd* virus in an electrostatic cage. Other acting factors that can influence transition points include van der Waals contacts, hydrogen bonds, electrostatic forces, the depletion process, and steric hindrance.

3.2. Interactions Affecting LCs. Colloidal definition applicable to nanosized particles such as CNCs is extendable to larger microphases such as "tactoids". Similarly, tactoids with

a surface charge are envisionable, which can have charges due to the dissociation/ionization of surface groups and the adsorption of charged molecules/ions in aqueous environments of individual CNCs. In the case of salt added, a cloud of counterions forms around the particle, balancing and screening the surface charge.[43] Whenever identical nanoparticles are arranged in double layers and overlap, osmotic pressure causes a repulsive force to arise. The size of the energy barrier, U, or more accurately the contact potential between the particles, U, controls how stable a colloidal system is.

Knowing particle diffusion inside the solution or how other particles impede particle mobility is crucial, in addition to revealing particle interaction strength. One notable factor is concentration. According to Doi and Edwards' hypothesis, the concentration regime may generally be divided into diluted, semidiluted, concentrated, and nematic regimes.[39] In the diluted zone, particles can easily spin while meeting one another. In the semidilute zone, it is difficult to spin particles without causing them to interact with one another. The CNC network makes both particle rotation and translational motion troublesome in the concentration regime. Therefore, there is a point at which "tactoids" also interact.

If colloidal particles are not networked, they are often of little use in soft matter design. To produce jammed or gelled states with improved mechanical qualities, rod suspensions are frequently made at a concentration that permits prolonged rod contact. It is related to attraction strength indirectly: if attraction capacity is effectively zero (repulsion), the system with increasing particle concentration levels achieves a glassy state; otherwise, a gel is formed. The jammed or glassy state is the kinetic stalemate of the framework, whereas the gelled state is the structure created after aggregation. Charge, dispersion, depleting forces, and friction contacts[44] may all have a precise and detailed impact on rod contacts; therefore, it is crucial to understand the mechanisms that lead to particle gel formation or kinetic standstill. The structural variation of a rod network is determined by this type of interparticle interaction. It is possible to create structures ranging from noninteracting rod networks to fractal clusters with rods; the same rationale is applicable to "tactoids".

3.2.1. Depletion Mechanism. An essential tool for researching the basics and real-world issues in soft matter physics is the capacity to modify colloidal particle interactions from short-range repulsion to short-range attraction. The issue is closely connected to current and recent studies on clustering and stability,[45] dynamical arrest,[46] and gelation.[47] One way of tuning interactions is to use depletion. The Asakura and Oosawa coarse-grained depletion model is the most well-known to describe such systems.[48] In this model, the polymer-to-colloid size ratio and polymer concentration may be changed to adjust the potential's range and strength.[49] In the remaining sections of the manuscript, tuning depletion forces is used as a helpful strategy to adjust the chirality of CNCs to achieve a red-to-blue shift and adjustable optical behavior.

Both water-soluble polymers and mixed particles in CNC solution have the potential to cause depletion. A Pickering emulsion of oil in water was stabilized by depletion in recent research using cellulose nanofibrils (CNFs), which were generated via surface adsorption of CNCs.[50] Nonadsorbing CNF[50] initiates this depletion effect. According to one author, bacterium depletion flocculation can be facilitated by CNCs;[51] once more, two morphologically mixed noninteracting particles cause depletion. Lekkerkerker and Tuinier[52] reviewed the extensive theoretical studies on the function of hard spheres, hard rods, and thin discs as depletants given the dearth of experiments. A potent technique for changing liquid crystal structure and CNC pitch is depletion contact.

4. LIQUID CRYSTAL FORMATION OF CNCS

This chiral nematic structure of CNC-based films offers outstanding optical capabilities due to its photonic crystal nature. The rainbow color and birefringence properties were achieved by the structure's arrangement of chiral nematic LCs. The tobacco mosaic virus,[53] cylindrical viruses (*fd* and *M13*),[54] DNA fragments,[55] poly(tetrafluoroethylene),[56] flagella filaments,[57] collagen,[58] boehmite,[59] cellulose,[60] chitin,[61] κ-carageenan,[62] synthetic polypeptides (polybenzyl-L-glutamate (PBLG)),[63] and polysaccharides (xanthan and schizophyllan)[64] have all been observed to undergo LC phase separation based on excluded volume effects. Remarkably, all these substances exhibit structurally colored iridescence, with physically stemmed coloration displayed only by the arrangement of such structures. The research done on any of these materials can be used for CNCs and CNC materials that have chiral nematic architecture. Not all chiral chemicals produce cholesteric phases, and nematic phases, such as the tobacco mosaic virus, are usually identified exclusively in elongated inclusions (CNCs). Chiral structures have helices; most of these helices have a fluted shape and a high electric charge. How molecular chirality presents itself in the macroscopic characteristics of the chiral phases formed and what intermolecular interactions are involved are unknown.[65]

Onsager's hypothesis[35] states that networks of long, rigid rods interacting with only repulsive forces result in an orientational (or nematic) pattern at a critical density that is far from maximum packing. Studies for rod viruses were first undertaken, but in 1959 Marchessault et al.[66] reported CNCs, a rod-like particle related to rod viruses, and this opened the door for cellulose study in LCs. In 1976, Gray et al.[67] reported that hydroxypropyl cellulose, which is composed of stiff polymer chains resembling rods, may also produce chiral nematic LCs at small doses. Revol and associates reported decades later that raw materials derived from cellulose may create stable lyotropic chiral nematic liquid crystal phase structures.[68,69]

Nematic layers, with the directors turning slightly as the structure progresses, make up cholesteric liquid substances. The distance required to complete one full circle of the director is known as the pitch length, which is important for building helical structures. Pitch length, one of the most crucial pragmatic factors that has been the focus of much research, distinguishes the cholesteric mesophase. This classification is self-evident since pitch length in some chiral systems is on the same order of magnitude as visible-light wavelength. These systems display intriguing optical characteristics because of their pitch existence, including Bragg reflections and reduced laser emission,[70] which have been used in many optical applications.[71]

Pitch length can be measured by looking at the peak of reflected light, or it can be directly observed using polarized optical microscopy (POM) or scanning electron microscopy (SEM); POM, however, is not very accurate. Pitch length recorded with SEM is substantially shorter than pitch length recorded using POM, according to the authors of one study. The CNC chiral photonic material pitch therefore cannot be expressed solely using the POM pitch, albeit it is helpful. An optical microscope can show a variety of stripes because of interference fringes, varying undulations, and helicoidal quasi-layers in an oblique orientation. As a result, the fringe pattern of
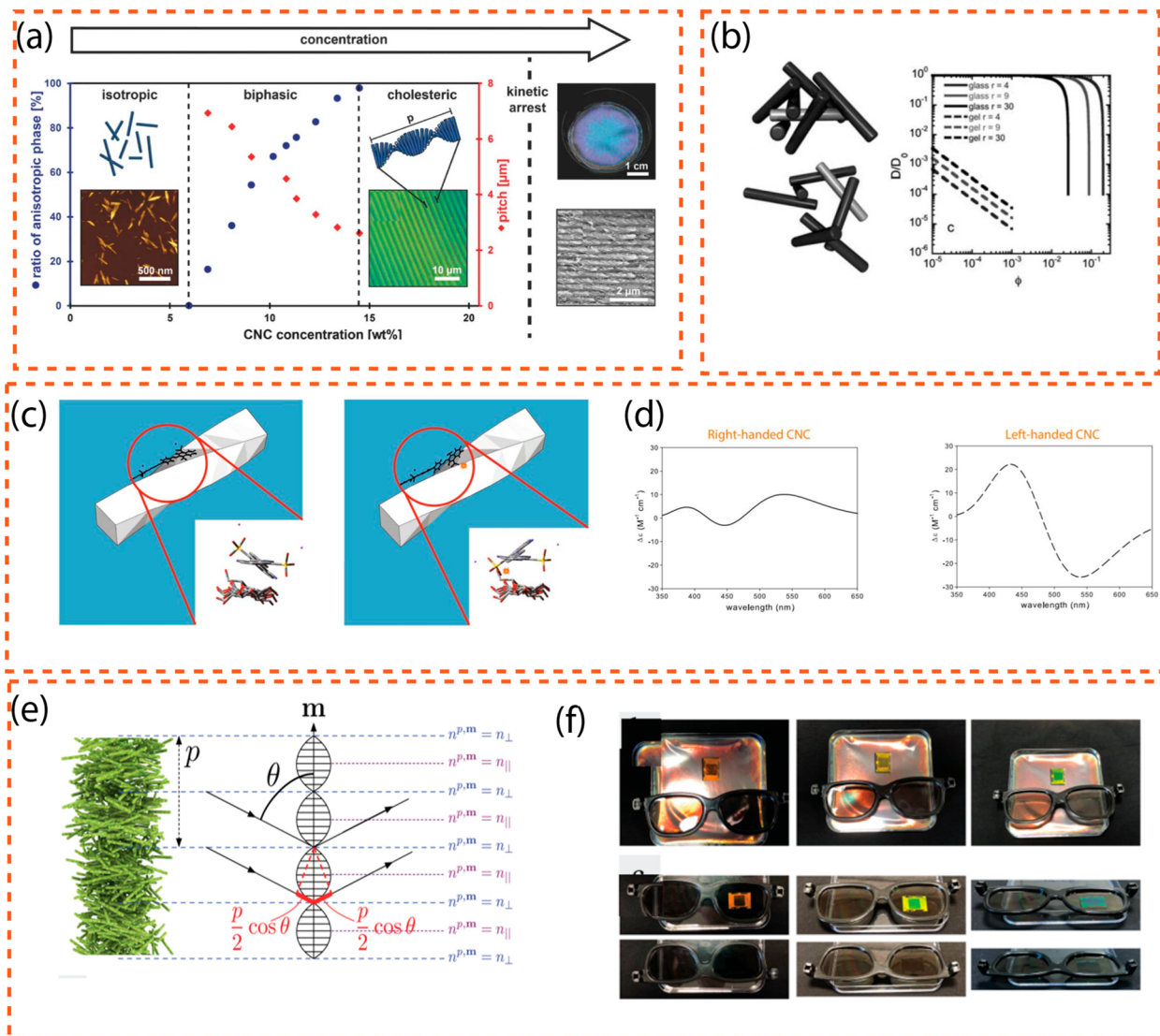
Figure 2. Chiral structure of CNC suspension. (a) CNC suspension self-assembly during evaporation to create an architecturally colored sheet (without the addition of dye or pigment). AFM images of individual CNCd are shown with the phase diagram, which shows the shift from the isotropic to the cholesteric phase when CNC concentration rises (blue dots) and the associated equilibrium pitch (red diamonds). Polarized optical microscope images of a common cholesteric phase fingerprint pattern are also shown in the upper corner. Adapted with permission from refs 97 and 98. Copyright 2016. Wiley-VCH, American Chemical Society. (b) The influence of the suspension structure on rod dynamics. Based on the ideas of Edwards and Evans[83] and Krall and Weitz,[84] the volume-fraction-dependent self-diffusivity of rod suspensions is computed, and the diagrams show how the CNC dynamic changes with volume fraction and charges. Adapted with permission from ref 99. Copyright 2010. Royal Society of Chemistry. (c) Circular dichroism of Congo red was induced on a twisted CNC. The top two Congo red enantiomers, A (+) and A (−), interact differently with the chiral nanocrystal surface. The A (+) enantiomer and the right-handed surface have a steric interaction on the right. The enantiomeric ratio changes due to favorable interactions between the conformation on the left, A (−), and the right-handed surface. The cartoon is not scaled. (d) Bottom CNCs with a right-handed twist bind Congo red preferentially in an orientation that generates a positive Cotton effect. Left-handed CNC cause a negative Cotton effect. Adapted with permission from ref 85. Copyright 2017. Springer Netherlands. (e) Application of Bragg's law onto the chiral structure of CNCs. Adapted with permission from ref 100. Copyright 2020. Multidisciplinary Digital Publishing Institute. (f) Circular dichroism of CNC chiral structures explored with circularly polarized glasses. Adapted with permission from ref 100. Copyright 2020. Multidisciplinary Digital Publishing Institute.

liquid crystals is confused with these comparable inter-references.[72]

Gray and colleagues[68] described for the first time in the research that permanent chiral nematic phases may be generated from stiff rod-like CNC suspensions made from natural cellulosic materials. Above a certain concentration, ordered chiral nematic phases naturally emerge, with the biphasic regions' identifying tactoids. These tactoids are spherical, ellipsoidal, or spindle-shaped droplets that are subject to hydrodynamic forces and have a propensity to coalesce into uninterrupted anisotropic phases.[73] According to the paper, this

helical configuration of CNCs has a pitch that is in the tens of micrometers range when it is fluid but decreases to sizes below 1 μm when it is dried, causing Bragg reflections of visible light from dried films that have a photonic band gap with an iridescent color.

Reading the literature demonstrates that, like the individual CNCs that existed before "tactoids" developed, chiral organization in colloids is impacted by physics and fluid dynamics. Self-assembled CNCs' surface charge density (i.e., the amount of sulfur present) and ionic strength, together with size and size distribution, all affect the chiral nematic pitch of the

particles. For instance, in CNC suspensions formed of wood pulp, when CNC length drops, so does the pitch of the chiral nematic phase. The chiral nematic structure's pitch size in solid CNC films is influenced by several factors, including the starting solution concentration, media ionic strength, and drying circumstances. Recent desulfation research has shown that higher sulfate concentrations increase the pitch values in solid films (effect of sulfate content or surface charge on the pitch); sulfuric dosage, temperature, and time all affect sulfur content.[14]

Here are some numbers from a recent study.[74] The mean pitch size fell from 15 to 2 μm as the vol % climbed from 2.5 to 6.5; however, the spacing between CNCs increased from 51 nm at the beginning of anisotropic phase growth to 25 nm above 6 vol % (completely liquid crystalline phase). According to the researchers, when the volume percent increased from 2.5 to 6.5 vol %, the twist angle between adjacent CNCs increased about from 1° to 4°. The rise in magnitude of the repulsive interactions between both the charged rods as the mean distances and angles lowered was related to the twisting's dependency on the volume fraction. Previous studies have assessed pitch values associated with CNCs as varying between 10 and 60 μm, but nothing is understood about how the pitch altered with volume fraction.[69,75−77] Therefore, particle concentration influences CNC chirality.

The research is also awash with information on which factor affects CNC chirality more—surface charge or twist. Revol and Marchessault claim that the CNC chiral nematic liquid crystal phase[68] was produced as a result of the twisted spiral shapes. Further research by Orts et al.[78,79] revealed that the CNCs in the aqueous phase had a distorted spiral rod-like shape, as shown by in situ small-angle neutron diffraction. Araki and Kuga[80] identified CNCs from bacteria in 2001.

However, chiral nematic liquid crystalline structure did not develop when the electrolyte was added to the solution. They proposed that the flat cylindrical form changed into a twisted rod shape when the electrolyte was added, resulting in a lower effective particle size. In particular, the rod shapes were inclined. Therefore, the spiral-nanorod form of CNCs plays a crucial role in the creation of chiral nematic LCs. Bacterial cellulose was hydrolyzed in sulfuric acid to form the rod-like microcrystal solution, which was subsequently separated into nematic phases by dialysis. The solution's phase separation behavior was altered by the addition of salt, which led to its transformation into a chiral nematic structure. This behavior shows that the chirality of the particles, which is protected by repulsive forces,[81] originates from their twisted shape. This perspective could be accurate since the tobacco mosaic virus (TMV) generates chiral structure and possesses structural chirality and intrinsic asymmetry as well.

Figure 2a shows the CNC suspension self-assembly process during evaporation to generate a functionally colored film (without the addition of dye or pigment). The phase diagram depicts the change from the isotropic to cholesteric phase (blue dots) as the CNC concentration increases, as well as the accompanying equilibrium pitch (red diamonds); it is supplemented with atomic force microscopy (AFM) pictures of individual CNCs. In the top right corner, polarized optical microscope photographs of a typical cholesteric phase finger-print image are also exhibited. Because the helical axis is orthogonal to the film, no fingerprint texture areas can be seen if the CNCs in chiral photonic films are parallel to the surface of Petri dishes. "Tactoids", on the other hand, expand and merge by a coalescence mechanism as the CNC self-assembles to create a

chiral nematic film. Faults from failed "tactoid" fusing persist in the CNC chiral photonic films, giving in a plethora of distinct fingerprint characteristics visible under POM.

According to hypotheses, the slowdown interactions of these two states vary very sharply because slow dynamics appear in a very narrow volume fraction range for glasses, and it shortens as aspect ratio is increased. Figure 2b shows the contrast among nanoparticle kinetics and volume fractions for glass and gel states (here denoted by r as the ratio of length over diameter). These representations were slightly altered when polydispersity was included in the equations. Exploring glassy or gel states is vital when scientists wish to lock in liquid crystalline formations in films, in addition to offering a practical method for changing the characteristics of CNC.

To lock in the liquid crystal structure, one may resort to adding coagulants. Aggregation is a thermodynamic balance between the energy required to keep particles in the aggregation state and the energy required to disperse them through thermal movement of water molecules. On the other hand, if the energy barrier falls below a certain threshold, aggregation will start. In this stage (coagulation), CNC particles/tactoids adhere and, depending on concentration, collapse or create a 3D gel readily,[82] the dynamic of which is explained by theories.[83,84] Later in the rheomechanical section, it will be demonstrated how the presence of a coagulant causes partial melting of LCs.

Recently, ref 85 used optically inactive Congo red produced circular dichroism to assess the structural chirality of CNCs (as depicted in Figure 2c and d). Conventional wood CNCs are expected to be 800 nm per half-twist right-handed, which is compatible with directly measured twists.[10,86] Imaging the twist is problematic due to the small lengths of wood-sourced CNC (100−200 nm), and tiny structural faults generated by such a twist would be difficult to discern using diffraction methods. The dye probes the crystal's surface, allowing these tiny character-istics to be quantified. Dong and Gray[75] accurately hypothesized that the positive "Cotton effect" was created by a right-handed twist of the CNC, but the reason could not be identified without a computational investigation at the time. Recent observa-tions,[10,86,87] as well as molecular models,[85,88] show that CNCs have a right-handed twist and that the cellulose crystal structure is more complicated than a flat crystal. As a result, it is reasonable to assume that the twist related to the structural chirality of CNC influences their capacity to separate, template chiral materials, or conduct chiral catalysis, as well as direct particle interactions at greater concentrations. These theoretical conclusions are compatible with the morphological findings of Usov et al.,[10] who used AFM to show evidence of right-handed chirality on both bundles and single fibrils.

Due to the creation of "coffee rings" during solvent evaporation, the CNC chiral optical film has a circular iridescent structural color and is narrower in the center and broader at the boundaries. According to Bragg's rule, the structural colors of CNC chiral photonic films are angle-dependent, which is a common property of structural colors,[60] which were previously classed as angle-dependent and independent. As the angle of incidence of natural light decreases, the color of CNC chiral photonic film changes from red to blue; alternatively, when the angle of incidence is fixed, the color of CNC chiral photonic films depends on the pitch of the CNC chiral nematic framework and its helical axis orientation relative to the film normal.

The wavelength of the reflected light that produces the color transition[89] is governed by the pitch of the LC, which is indicated by the letter P in most literature, a fact validated by

Dumanli et al.[90,91] on a CNC-based LC film. The reflected wavelength is defined by the Bragg[92] equation, $\lambda = nP \sin(\theta)$, where lambda is the reflected wavelength, P is the helical pitch, θ is the incoming light's angle, $\sin(\theta) = 1$ when the incident light is perpendicular to the crystal plane, and n is the material's average refractive index.[93] Dumanli et al.[90,91] reported that pitch predicted by the Bragg equation agreed visually with experiments. As a result, the photographs acquired with a polarized optical microscope (POM) below may give reliable proof for the cholesteric LC[94] as shown in Figure 2a. There are approaches in the literature for making unnaturally architecturally colored colloids angle independent; however, these studies are beyond the focus of the current study. As previously stated, Bragg's rule may be applied to CNC chiral character, indicating how such a structure interacts with incoming light; moreover, the CNC chiral structure reflects left-handed circular light but transmits right-handed circular light; these changes are represented in Figure 2f. Instead of measuring the absorbance of isotropic light, circular dichroism (CD) spectroscopy compares the absorption of right-handed and left-handed circularly polarized light by a material.

As a result of the salt addition, the critical concentrations for the anisotropic phase rise, and the boundary between both the isotropic and anisotropic phases blurs. As the salt concentration was increased (the concentrations in the two phases become more similar), the limit between the phases becomes more diffuse, and as a result, the isotropic phase exhibits some birefringence between cross polarizers, making calculating the volume fraction of the phases more difficult. This finding was connected in the literature to a shift from a first-order transition, which should appear as clean phase separation, to a second-order transition, where critical fluctuations are involved, and the transition seems to be delayed. Moreover, even in the absence of sufficient salt, increasing the concentration of CNC (obtained by sulfuric acid hydrolysis) boosts the ionic strength of the suspensions since CNCs are surface charged, rendering separation difficult to quantify at high CNC concentrations. Furthermore, the addition of salts lowers the effective diameter of the CNC rods, leading to an increase in aspect ratio and a decrease in effective volume (and hence the effective volume concentration of the rods in the suspension).[95]

Changes in ionic strength can affect pitch length as well as transition points. Shafiei-Sabet et al.,[96] for example, dispersed CNCs in deionized water or NaCl solution to modify the pitch of the systems. According to the Derjaguin–Landau–Verwey–Overbeek (DLVO) hypothesis, the equilibrium between these electrostatic and van der Waals forces drives the instability of colloid suspensions. As a result, DLVO theory allows one to substitute the original aspect ratio of rods with an effectively decreased aspect ratio (allowing for electrostatic repulsion range) and input it into Onsager theory to discover the point of transition from isotropic to nematic, and so on.

In the low-salt limit, more charges interact efficiently further away from the spiral–spiral contact, resulting in helical axes that are aligned perpendicularly. The SAXS and laser diffraction measurements reveal how the average distance between the CNCs and pitch values changes when volume fractions (or charges) change. The angle one rod must twist is in its neighboring vicinity, assuming that $\theta(\varphi) = 360 \frac{d(\varphi)}{p(\varphi)}$. The twist is related to the competition for total energy between entropic and enthalpic contributions. The enthalpic contribution from rod–rod interactions becomes significant when the space

between rods is short, i.e., when CNC concentration is high or salt is added. It is critical to accurately estimate these two contributions because attractive interactions stimulate parallel orientation while Coulombic interactions encourage orthogonal orientation.

A significant number of negative sulfate groups on rod-like CNCs hydrolyzed by sulfuric acid always cause electrostatic repulsion,[1] permitting the production of stable chiral nematic mesophases (liquid crystal formation is salt-dependent). The repulsive forces between CNC rods are too large to allow CNCs alone to assemble into a chiral structure when treating CNC suspension as an ion-free media and comparing the findings to the DLVO theory; however, this is charge dependent as desulfation through the application of heat might lead to the easier formation of chiral structures.[101,102] Indeed, CNC suspensions treated with long-term water dialysis to remove counterions have a high zeta-potential value and exhibit achiral nematic characteristics; desulfation in this case can act in reverse. When this CNC suspension was dried into a solid film, no iridescent hue was noticed, and no peak in the ultraviolet (UV)−vis spectrum was observed.

By screening the surface charges and reducing the steric effect, salts and polyethylene glycol (PEG) (nonabsorbing polymer) can also minimize repulsion.[103] The interaxial lengths between CNC rods were estimated by determining the peak position in the SAXS curves to be smaller in salt (44.0 nm) and PEG (45.6 nm) systems compared to the original clean system (48.7 nm).[74] By reducing pitch size, reducing interaxial separation, and raising interaxial tilt, adjacent CNC particles' chiral nematic structure is maintained after drying, and the associated films display iridescence. In one trial, oxalic acid rather than sulfuric acid was used to treat CNCs. Oxalic acid was used to discover the CNC film's brilliant snowflake-like pattern rather than sulfuric acid. More significantly, carboxylated CNCs produced by oxalic acid readily formed a LC phase by adding the cationic solutions to 1.27 wt % CNC solution.[104] In brief, the chirality of the CNC suspension and films may be altered by manipulating colloidal forces; this repulsion can be controlled by altering charges or introducing a small quantity of coagulant.

Figure 2d shows that the CNC chiral photonic film has markedly sunnier iridescent structural color schemes when lighted to left circularly polarized light (L-CPL) than when lit up with unpolarized natural light, and it is almost translucent when lighted with right circularly polarized light (R-CPL). Nevertheless, with R-CPL, CNC chiral optical material has no discernible troughs. Under L-CPL, the four areas of CNC chiral photonic film have much lower transmittance than ambient light in their respective valleys, resulting in enhanced contrast and brighter iridescent colors. According to these results, the CNC chiral photonic films exhibit chiral nematic structures that are left-handed.[105,106] Figure 2f shows these evolutions visually with circularly polarized glasses.

4.1. Coassembly of CNC and Other Nanoparticles.
Nanoplasmonic and photonic crystals work together to provide innovative optoelectronic properties that have the potential to lead to the development of better materials and gadgets. Anisotropic gold nanorods and rod-like CNCs may be combined to form free-standing chiral−plasmonic composite films, which have the potential to exhibit chiroptical-modulated activity over a wide range. Surface plasmons, which may confine light to a subdiffraction-limited area and dramatically improve light−matter interactions, can be sustained by metal nanoparticles (in this case, gold nanorods). A design of chiral

plasmonic hybrid films created by fusing gold nanorods and CNCs is shown in Figure 3a. Because the negatively charged
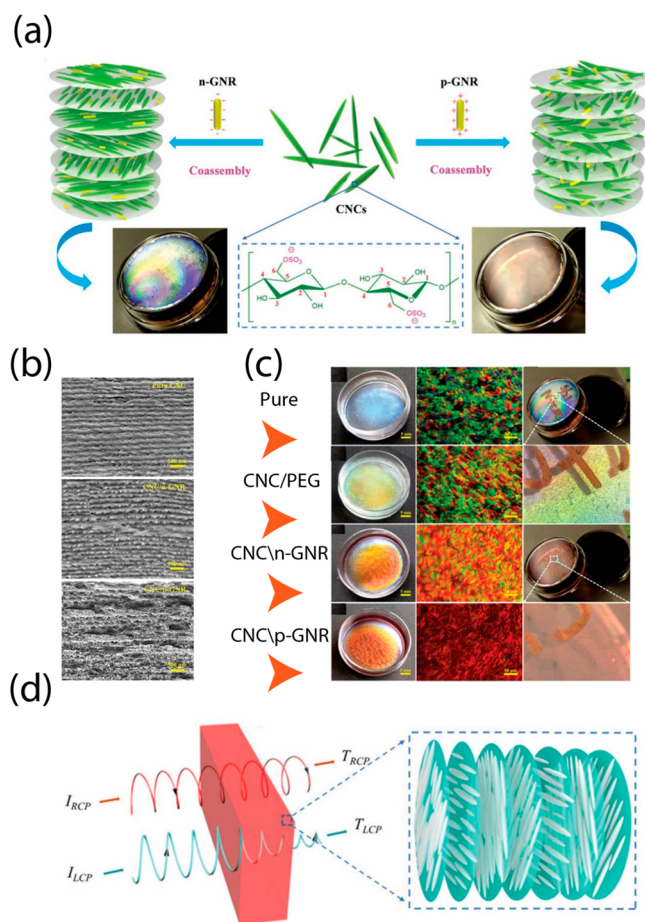

Figure 3. Coassembly of CNCs with other ingredients. (a) Schematic of the hybrid chiral plasmonic films made from charged GNRs and CNCs. The negatively charged gold nanorods were distributed evenly and parallel to the CNC rods. The chiral nature of CNCs is maintained. The positively charged gold nanorods are dispersed at random and aggregate in part. There have been reports of CNC nanorod gelation and flocculation with some chiral nematic ordering perturbed. Adapted with permission from ref 107. Copyright 2019. Wiley-VCH. (b) SEM of cross-section images of pure CNC, CNC/n-GNR hybrid film, and CNC/p-GNR hybrid film. Adapted with permission from ref 107. Copyright 2019. Wiley-VCH. (c) Photographs of pure CNC film, CNC/PEG film, CNC/n-GNR film, and CNC/p-GNR film in liquid and dried forms. Adapted with permission from ref 107. Copyright 2019. Wiley-VCH. (d) Diagram showing the path of circularly polarized light through a left-handed chiral-structured CNC film. Passive left-handed circular polarization light is produced by the chiral photonic film's preferential reflection of incident light, whereas passive right-handed circular polarization light is transmitted. Adapted with permission from ref 107. Copyright 2019. Wiley-VCH.

gold nanorods were arranged uniformly and parallel to the CNC rods, the chirality of the CNCs was maintained. The chiral nematic ordering is somewhat broken as a result of positively charged gold nanorods being dispersed randomly and forming a partial agglomeration.[107] Cross sections of pure CNC and CNC/n-GNR hybrid films are depicted in SEM pictures in Figure 3b. As can be observed, the pitch sizes of the CNC/p-GNR hybrid film are all twisted; however, the CNC/n-GNR hybrid film is unaffected, just like pure CNC film.

As shown in Figure 3c, four different types of chiral-structured iridescent composite sheets were produced by gently evaporating water for 2 days at 30 °C and a RH of 80%. The pristine CNC films have a prominent blue color with several iridescent color zones because of the chiral structure's helix orientation. Remarkable are the clear pure CNC films' photonic crystal properties and vivid iridescent chiroptical activities. Due to the steric stabilization produced by PEG, the CNC-PEG film reflects yellow principally with a small red shift observed in comparison to the CNC film. Surprisingly, the presence of gold nanorods causes a large red shift to be seen. While there is no agglomeration and a more uniform color on the CNC/n-GNR hybrid film, this is not the case on the p-GNR hybrid film. Because of electrostatic interactions, p-GNR will prevent CNC from forming a chiral nematic structure, but n-GNR, which is present at the same concentration, is dispersed uniformly inside the helix conformation and encouraged to do so.

The pure CNC film shows significant birefringence and multidomains with variable sizes and orientations because of the lack of control over helix alignment during evaporation. PEG incorporation hardly modifies the domain color but has no discernible effect on the appearance of birefringent and "fingerprint" textures. On the POM pictures, the as-prepared CNC/GNR composite films show a progressive transition in the domain color from brilliant green to dark red. The CNC/n-GNR hybrid film exhibits a more constant iridescent color than the CNC/p-GNR film. According to the seeming flat appearance, the structured helix patterns are all still present in the solid sheets (spaced parallel lines). The fingerprint texture pattern of the CNC/n-GNR hybrid film is cleaner and more organized when compared to pure CNC and CNC/PEG films. The fingerprint texture pattern is less distinct and more blurry on the CNC/p-GNR film.

Due to their left-handed helical shape, chiral cellulose films may selectively reflect and transmit incoming light to produce circularly polarized light (CPL) with opposing helicity states.[105] The inherent capacity of chiral cellulose materials to convert incoming light into passive left-handed CPL (L-CPL) through selective reflection and passive right-handed CPL (R-CPL) through transmission is shown in Figure 3d. There is a distinction between L-CPL and R-CPL in terms of absorption.

Xu et al. noted that the interlamellar splitting and self-assembly process among graphene oxide (GO) suspensions (an LC-forming suspension) in nematic or lamellar phases can be synchronized by the addition of hydrophobic substances like silica nanoparticles via an entropy-driven depletion mechanism.[108] Another method for generating depletion forces in each system is to utilize a polymer that does not interact with CNC particles. If macromolecules do not adsorb at the particle interface, the exclusion of polymer segments from particulate volumes results in an effective entropic pull between particles known as depletion interaction. The anionic polyelectrolyte carboxymethyl cellulose (CMC) has greater osmosis over nonionic polymers at the same molecular mass, as reported in ref 109. This is because the increased radius of gyration brought on by intramolecular charge repulsion makes CMC an anionic polyelectrolyte. Because anionic CMC chains do not adsorb on them, they can promote depletion-induced self-assembly CNC nanoparticles, according to the literature. Nonadsorbing micelles, such as those used in protein crystallization, can likewise induce depletion pressures on CNC particles. The inclusion of nonadsorbing compounds in the suspensions causes these difficulties.

4.2. Parameters Influencing Chirality. Pure hard rod CNC suspensions, as previously mentioned, exhibit remarkable phase transitions. The inclusion of nonadsorbing polymers as depletants influences these transitions; these additives have a considerable effect on the isotropic−nematic (I−N) phase transition of CNC suspensions.[52,110] Depletion effects may be used to change colloidal stability, expand the coexistence of regions in I−N transitions, and fine-tune the angle of twisting of chiral structures. Scientists in the literature were startled by depletion effects since adding a nonadsorbing polymer resulted in the stabilization[111] of graphene oxide suspensions rather than the predicted instability. Furthermore, the viscosity of the suspension was lowered by many orders of magnitude.[111] The formation of smectic fibrils at intermediate depletion strengths resulted in a polymorphic shift from two-dimensional crystalline monolayers at mild depletion to one-dimensional columnar fibers at strong depletion;[112] the agent's concentration and molecular weight can be fine-tuned to fine-tune the strength of depletion. The usual growth period, according to the author, differed by more than 6 orders of magnitude, needing days for big platelets to mature, minutes for smectic fibrils to develop, and milliseconds for columnar fibers to form. Aside from the fundamental rod−rod contact (thermodynamic), kinematics plays a significant role in the structure's creation.

Depletion can also be caused by other nonabsorbing noninteracting nanoparticles, as was previously described. When dextran, a depletion agent, is introduced to the biphasic zone, the coexistence (isotropic and nematic phases) region is greatly increased. The isotropic phase is where dextran preferentially divides. After solidifying the CNC/PEG and CNC/salt suspensions, the interaxial angle between CNC rods widened. The interparticle distance was simply connected to the salt content; however, it was shown that the angle depended on both ionic species and ionic strength as explained in terms of interaction energies. CNC films made by suspension casting have been demonstrated to create left-handed chiral nematic structures that polarized incident light and reflected left-handed light.[113] Simulations show that a mixed particle system, like the GO dispersion and silica nanoparticle used in ref 108, can similarly activate depletion mechanisms.[114] The depletion interaction and its influence on distinct colloidal particles with diverse geometries are thoroughly explained in ref 115. DNA can also cause the clay liquid crystalline part to swell.[116]

Finally, the addition of polymer lengthens the pitch in some circumstances and generates a red shift in the light that is reflected; this happens in scenes where the polymer is located between CNC rods and pushes the sheets apart, lengthening the pitch. The variety of characteristics has an impact on the degree of red shift such as flexibility, rigidity, the radius of gyration, and binding between the polymer and CNC rod;[117] on the other hand, nonadsorbing polymers[118] or polymers with low molecular weight[103] act as depletion agents, and pitch size decreases as polymer concentration increases. Widening the reflection spectrum appears to be essential for the development of broadband applications to produce novel photonic crystals. Authors[119] generated films of CNCs that exhibit circularly polarized reflection throughout the visible spectrum (broadened) using micelles. The optical characteristics of additional chiral nematic LCs, which are now utilized extensively in display technologies,[119] may be modified using this innovative technique. Micelle helped in the process of self-assembly that causes CNCs' cholesteric stage to deform.

To describe the procedure, "tactoid" formation—a process similar to crystallization in polymers—occurs when the solvent evaporates, the loading of CNC rises, and "tactoids" form.[120] A constant film with chiral nematic order results from the tactoids' fusion and deposition. Nevertheless, because micelles are present, they become caught in the CNC's liquid crystal domains' developing lamellar structure and prevent the domains from merging into long-range homogeneous structures. Authors hypothesized[121] that the accumulation of the micelles between cholesteric domains is due to the exclusion effect of dense LCs on large-size nanostructures.[122] Additionally, at the micelle−liquid crystal phase contact, these micelles show a reorientation impact on the LC mesogens that precludes the flat alignment of CNCs in each stratum. The micelles cause the domains in the film to tilt as compared to the usual horizontal deposition direction brought on by gravity. The micelles, however, collapse as the CNCs continue to dry, leaving a heterogeneous CNC film.

In contrast, soft polymer molecules can intercalate into the cholesteric phase of CNCs to generate a homogeneous film[123] when water-soluble polymers or melting elastomer latex is used. Finally, CNC lyotropic chiral nematic LCs were deposited into CNC films with considerable disorder due to submicrometer-sized micelles produced by an anionic surfactant. Chirality has a relationship with CNC polydispersity as well. According to Lekkerkerker and Tuinier,[52] large biphasic range development is a direct result of CNC polydispersity and has been found in other polydisperse rod-like colloidal suspensions as well. For example, graphene oxide suspensions display comparable behavior, and the authors observed that the biphasic suspension's compositional range was extremely large due to platelet polydispersity.

As a final note explaining the difference in chiral behavior of CNCs on nonadsorbing and adsorbing polymers, the addition of polymer increases pitch length in some circumstances and creates a red shift in the reflected light, and the polymer chains are implanted between CNC rods and increase the CNC interaxial distance. The degree of red shift is determined by key characteristics such as flexibility, rigidity, the radius of gyration, and binding between the polymer and CNC rod;[117] on the other hand, nonadsorbing polymers[118] or polymers with low molecular weight[103] act as depletion agents, and pitch size decreases as polymer concentration increases.

To summarize, pitch length varies with salt and CNC concentration, and fractionation due to centrifugation or phase change results in shorter or longer rod separation; this fractionation results in an increase or decrease in pitch size.[124] Whenever repulsive contacts are adjusted, such as screening charges with salt or reducing surface charge via healing, pitch length is decreased. Swelling stretching causes an increase in pitch size, and compression provides a reduction in pitch size.

4.3. Orientation. Liquid crystal arrangement and direction are equally important and demand particular study. SAXS and small-angle neutron scattering (SANS) scattering have also been used to some extent to examine the structural characteristics of the ordered chiral nematic CNC phase. According to SANS data, CNC rods in chiral nematic suspension that is magnetically or shear aligned are packed more densely parallel to the chiral nematic axis than perpendicular to it.[78,79] Additionally, Orts et al.[78,79] have demonstrated that rod spacing reduces as CNC concentration and added electrolyte content increase. Until now, attempts to control CNC director orientation have only used external fields, shearing, and the use of electrical or magnetic fields, all of which have varied degrees of success.

Fibers with diamagnetic anisotropy align under static magnetic fields. Carbon fibers,[125] carbon nanotubes,[126] polyethene fibers,[127] cellulose fibers, and so forth undergo magnetic alignment. The experiments in which liquid crystalline fibers of these comparable rods are magnetically aligned can be simply expanded to CNCs. Because cellulose fibers are diamagnetic, the chiral nematic axis aligns parallel to the static magnetic field, and several studies on chiral nematic phases formed from cellulose fiber suspension have been reported.[128] Magnetic field application is the only method reported thus far that can control the helix's direction. Although the literature has a footprint in using microfluidics to construct such structures, enhancing and changing orientation, particularly with relation to CNCs in their LC form, has not been recorded.

This method can deploy and position CNCs due to the negative diamagnetic anisotropy of CNCs, which have a rod directly proportional to the magnetic field. CNCs tend to align perpendicular to an externally applied magnetic field. The cholesteric phase may be aligned experimentally at modest magnetic fields ($\mu_0 H \sim 0.5 T$), allowing for angular control of the domains' helical direction.[129] Because the rods of a cholesteric CNC suspension are all perpendicular to the helix axis, when placed in a sufficiently powerful magnetic field, the helix will be uniformly aligned in the field direction. It has been empirically verified by Revol et al.[69] and Kimura et al.[130] that the magnetic field caused the parallel organization of a helical axis to the magnetic field direction, and magnetic field rotation (periodic) caused crystal unwinding as the suspension transitioned from liquid crystals to an isotropic state. Removal of the magnetic field also led to complete dissolution and relaxation of liquid crystalline phases.

Other observations involve the magnetic orientation of CNCs; literature searches indicate that magnetic fields have not been investigated for their impact on tactoid fusing. Furthermore, by observing its dispersion within the solution, tactoid nucleation may be made more homogeneous. Tactoid nucleation may be organized and studied similarly to polymer crystallization; thus, investigating ways to enhance or reduce it can be influential in the field. Although it did cause a disruption in liquid crystals in one study, a magnetic field was not employed to change the location of an isotropic to nematic or nematic to chiral nematic transition. Magenic fields' influence on tactoids' orientation can be paired with depletion forces. According to one account,[130] magnetic field alignment takes 5 h at 1 T; there are outstanding questions in this area regarding the influence of salt and depletion force or concentration on the rate of alignment and the effect they may have on accelerating or decelerating the rate of alignment. Paramagnetic nanoparticles, such as Fe_2O_3,[131] can also be painted onto particles to increase their sensitivity to magnetic fields and the pace of alignment. One study[132] found that altering a fluid's viscosity from water to n-methyl formamide (NMF) under a 0.7 T magnetic field might alter chiral orientation. The cholesteric with the least viscosity also showed the biggest rise in order prior to equilibrium and plateauing when the magnetic field was introduced. The greater viscosity suspensions, however, showed nothing after the first field influence in terms of temporal variations.

Viscosity has an impact on CNC ordering. CNC-water is more viscous than CNC-NMF. It thus struggles more to rotate in a magnetism. Since the rate of orientation is related to the solution's viscosity, CNC "tactoids" can be utilized as a probe for microrheological purposes. Similar to the fluorescence recovery after a photo bleaching probe,[133] this probe can provide information on the pore structure and degree of confinement of the area around the CNC "tactoid" probe. The rate at which different rods in distinct suspensions are oriented can potentially be a factor in "tactoid" variations.

Magnetic flux was also employed to create well-coordinated nematic liquid crystalline and liquid crystal specimens of virtually monodisperse TMV.[41] Onsager[35] developed a theory for the phase transition in LCs using TMV as well. When a nematic specimen is exposed to a magnetic field, positive diamagnetic (opposite to CNCs) anisotropic virus particles quickly align in the field's direction at an applied field of 22k gauss. When the field is withdrawn, the particles misalign once more, which is expected behavior for CNCs or rods with a similar structure. According to research, the pitch of CNC-based films reduces as the magnetic field strength increases. Both the pitch and the homogeneity of the film may be altered.

Habibi et al.[134] also used an AC field to generate highly directed low concentrations of CNC distributed in cyclohexane. The findings revealed that rod-shaped particles became parallel to the direction of the electric field rather than the magnetic field's orientation direction.[134] The authors used in situ small wide-angle X-ray scattering diffraction (SAXS/WAXD) techniques to study the GO nematic liquid crystal phase during polymer crystallization, concentrating on their hierarchical structure. It was reported that GO LC and polymer crystals coexist in the GO polymer complex, where polymer crystallizations influence the overall liquid crystallinity. While polymers crystallize in bulk or at the interface depending on the cooling rate, interfacial PEG crystallization on GO increases both GO alignment and PEG crystal orientation.

PEG with GO prefers to crystallize at the interface or in the bulk, depending on the crystallization kinetics, which ultimately influences the predominant direction of GO LCs. This work demonstrates another possible application of crystallization for ordering LCs.[135] To the best of our knowledge, no study has been published in the literature that reports on the ordering of CNC LCs employing polymer crystallization. Similar ordering through application of an electric field has been observed in clay suspensions;[136] similarly anomalous photothermal deformation of gels doped with uniaxially aligned nanosheets adsorbed with a dye is observed in one study. Only the colored portion of the gel is photothermally distorted when exposed to light.[137]

De France et al.[138] demonstrated that cooperative ordering favors field orientation. Magnetic fields of 0.56−1.2 T were insufficient to orient samples containing 1.65 and 4.13 wt % of CNC, a goal previously achieved for CNC made from tunicates.[139] They concluded that achieving orientation may necessitate a larger field, a higher CNC aspect ratio, and greater concentration. Using long CNCs, orientation was accomplished by untwisting the helix and, as a result, increasing the pitch size (red shift).[139] The procedure works best for suspension toward the low concentration size of the cholesteric regime that is accompanied by a minimum viscosity. It is also possible to create films with consistently oriented helices by beginning with a fairly low CNC content and progressively evaporating the solvent under a consistent magnetic field.

Considering the positivity of the dielectric anisotropy of CNCs, an electric field can act to unwind the helix. Habibi et al.[134] demonstrated a uniform CNC alignment in films obtained through drying CNC suspension in the presence of electric fields with moderate to strong frequencies. For the GO suspension, macroscopic orientation of LCs was reported to be readily tunable by an external field. However, an electric field widely

used for liquid crystal display switching is inapplicable to graphene oxide LCs. Under the application of an electric field, the negatively charged graphene oxide platelets underwent electrophoretic migration toward the cathode. After, the platelets accumulated at the cathodes and became electrochemically reduced. The authors suggested that instead of the application of an electric field a magnetic field or mechanical deformation is preferable to successfully control the alignment of crystals. Indeed, after prolonged annealing at room temperature under a magnetic field, shear-induced morphology disappeared, and a typical nematic "schlieren texture" emerged.[140] A group of sites where the director alignment is inconsistent define the "schlieren texture" of nematic LCs. These points correspond to disclination lines viewed end on. These "schlieren textures" are also visible in other liquid crystalline materials that display the texture stems from physics and superstructure as opposed to chemistry.[140,141]

Later, under the application of a strong magnetic field (0.25 T), induced alignment could be monitored; the domains with different liquid crystal orientations initially separated by disclinations were gradually reoriented and merged into larger domains. Due to the weak magnetism of the bare platelets, complete alignment took several hours. Decorating the platelets with iron oxide (Fe_2O_3) maintained the liquid crystallinity in an aqueous medium and completed field-induced alignments within several seconds under the same strength of the magnetic field. The liquid crystallinity of the suspension could also be maintained under mixing with a polymer matrix. Nanocomposites prepared with poly(acrylic acid) (PAA)/graphene oxide displayed birefringent schlieren texture under crossed polarizers. Under drawing by hand, and SEM, the authors found platelets to be highly aligned and stretched along the mechanical drawing direction.

Li et al.[142] reported photonic crystals with controllable structural color made from lyotropic graphene oxide solution using a simple colloidal self-assembly technique. They reported that graphene oxide with enormous flake sizes of roughly 2.4 μm had iridescent colors in certain configurations. After sonication, the structural color of huge flake size dispersion vanished, illustrating the importance of aspect ratio in the creation of photonic crystals.[142] It was also revealed that changing the GO concentration may easily modify the light reflected from the graphene oxide solution. One of the most effective ways of aligning GO dispersion is to use an electric field. Novel reflecting color display applications can be realized by combining the photonic crystalline ability of LCs with electrical alignment. Song et al.[143] did indeed create an electrically erasable and rewritable structured reflecting electrode design. The liquid crystal was manufactured of graphene oxide. By switching the direction of the electric field, writing and erasing may be done alternatively since color reflection only happens when the GO is parallel to the substrate. The change from darkness to light, however, happens exceedingly slowly. The likelihood of new GO liquid crystal suspension uses is anticipated to increase noticeably because of these photonic crystals.

The length across nematic planes all along the cholesteric axis is shorter than the length among rods in a nematic planes in a 2.4 T magnetic field when microfibril suspension displays asymmetrical chiral nematic organization.[78] A CNC from a microcrystalline CNC was employed in conjunction with poly(vinyl alcohol) (PVA) by Kvien and Oksman.[144] In that example, the authors claimed to have attained CNC alignment by using a 7 T strong magnetic field. They created transparent,

birefringent films of 90 μm thickness with a final concentration of 2 wt % of CNC (4.21 GPA) under these conditions and reported that it was significantly lower than the storage modulus measured in the transverse direction (6.19 GPA). This finding confirmed the idea that CNCs were perpendicular to the applied field.

Furthermore, the shear flow will provide uniaxial CNC alignment, which is another manipulation tool for directing the direction of the unwinding helix. Films with uniform nanorod alignment produced by shearing and X-ray study of liquid crystalline CNC alignment during shear flow revealed complicated behavior with significantly variable outcomes depending on shear rate.[145] The orientation of CNC in a microfluidic chip has also resulted in full orientation of individual CNCs,[146] but there is no report on orienting LCs in the same direction.

Other natural ways to arrange colloids have been documented in the literature. For example, grafting fluorescent dyes onto the ends of filamentous viruses produced a hydrophobic patch whose attraction could be adjusted by modifying the bound dye molecules. Increasing the tip attraction, according to computer simulation, stabilizes the smectic phase at the expense of the nematic phases.

The nematic state can be totally repressed for a direct isotropic liquid to smectic phase transition[147] if the tip attraction is strong enough. A similar strategy may be utilized to tune CNC particles if tweaking liquid crystalline formation or a specific LC phase of CNC is preferred over a common chiral nematic phase of CNCs. Performing an analogous experiment for CNCs and guiding the liquid crystal formation self-assembly process, on the other hand, may be tricky.

5. MECHANICAL PROPERTIES

CNC films are hard and brittle by nature. Brittleness is caused by the fact that CNC rods are inflexible and unable to relieve external stress through deformation, and there is no flexible connection between CNC rods other than hydrogen bonds, allowing fractures to develop easily.[148] CNC-based photonic materials can be produced to overcome these restrictions by assembly, postprocessing, or lamination with other nonbrittle components; for example, CNCs can be doped with weakly interacting chemicals that minimize brittleness while retaining structure formation. In the literature, this was done using a zwitterionic surfactant,[98] neutral or anionic polymer,[123] amino resins,[149] or sol−gel precursors and cross-linked latex nanoparticles.[150] CNCs with cholesteric layouts may also accept tiny nanoparticles such as plasmonic gold nanorods that enable complicated chiroptical effects[151] without altering the phase.[152] Weaver et al.[153] reported, via modeling and texture analysis, that a pitch of 75 μm can permit a variety of toughening processes that can inhibit fracture propagation.[153] Bouligand and colleagues[154] reported that the mechanical characteristics of natural high-performance biobased composite materials are derived from liquid crystal self-assembly, lending credence to their results.

The twisted plywood, or Bouligand, structure is the most prevalent microstructural motif in natural materials with high mechanical strength and toughness, including as bone and the mantis shrimp dactyl club[155] (see Figure 1). Similarly, the cuticle of lobsters[156] and other marine microorganisms[153] has remarkable fracture toughness, in addition to aesthetic characteristics. These materials are isotropically toughened by a low volume fraction of soft, energy-dissipating polymer and the

"Bouligand" structure itself via shear wave filtering and fracture twisting, deflection, and arrest. Because CNCs spontaneously self-assemble into chiral nematic films when cast from solutions, they are appealing candidates for bottom-up production of these structures. The ability to manipulate a material's nanoscale architecture enables fine-tuning of its physical characteristics and associated functionalities. Application of these structures in elastomers to produce an energy dissipation mechanism for increasing the toughness of composites is unexplored and recommended. Similarly in free-standing aerogels, tuning the chiral structure of the components increases the specific strength and toughness of CNC aerogels by up to 137% and 60%, respectively, which is equivalent to the greatest values recorded for cellulose nanofibrils or nanocrystals.[157] The resultant aerogels exhibit a significant link between the mesopore percentage and selective light reflection as a function of mechanical load (iridescence). The authors reported that chiral-nematic ordering considerably increases pore compression mechanical performance under load.[157]

The network of pore canals that helps toughen the material while simultaneously supplying components for self-healing is a crucial aspect of biological composites that has yet to be reproduced in man-made materials. CNC composites might be formed with or around a network of synthetic nano-/microconduits that help supply minerals or photopolymerizable monomers to damaged regions. These property improvement paths are still available and provide fertile ground for the development of CNC-based composites. The characteristics of the minority macromolecular phase in natural composites, which provides binding and energy adsorption, remain unknown. Most likely, these polymers are firmly packed in the nanoscale domains between the ordered mineral crystallites. As is generally known, the characteristics of a confined polymer differ substantially from those of a free polymer. The ordered, alternating arrangement of CNCs and polymers in CNC "Bouligand" composites, as well as the flexibility to change the CNC−CNC spacing, give an excellent opportunity to investigate natural polymer characteristics under confinement. Furthermore, the polymers used may be stimuli-responsive, allowing the "Bouligand" composites to be environmentally sensitive. The Bouligand arrangement has the greatest benefit for impact resistance and bending properties in carbon-fiber-reinforced composites. These characteristics for CNC Bouligand composites of films, however, have not been measured. As a result, more study in the field is required to overcome the uncertainties.

In practice, CNC has been mixed with polymers to increase mechanical properties like nature-inspired architectures. The incorporation of CNC films into larger laminar structures has been studied to achieve enhanced mechanical or optical properties. By inserting CNC films into the polymer, thin sandwiched structures with brilliant structural color, enhanced mechanical properties, and shape memory features were developed. Depositing CNC films onto either face of a birefringent membrane, similar to the jewel beetle chrysin resplendens,[158] enables simultaneous reflection of both left- and right-handed circularly polarized light. The sample optical mechanism was created by impregnating micrometer size planar gaps in CNC films with a nematic LC, producing a comparable birefringent layer that may be actuated by temperature or electric fields to change the reflected spectrum or polarization state.[159]

One method for improving the mechanical properties of CNC films is to mix them with water-soluble polymers. There are several methods for incorporating chiral photonic films into PVA or an epoxy resin; moreover, CNCs' inherent twist topology and uneven surface charge distribution make them easier to arrange into chiral nematic structures.[10] The critical concentration at which CNCs become anisotropic is defined by the aspect ratio and surface charge. During the phase separation and concentration produced by water evaporation, the tactoids rearrange and unite to form massive "tactoids", which is comparable to the Ostwald ripening process of emulsions.[73] According to the authors, the fusing of CNC "tactoids" is poor during rapid water evaporation, and only sections of the CNC film are in the liquid crystal structure as "tactoids" in the final CNC films. Water evaporation at the edge of a Petri dish happens quicker than in the core region due to the "coffee ring" effect, resulting in a mass shift from the center to the periphery. The exceptional mechanical properties of CNC chiral nematic LCs make sulfate CNC appropriate for research.

CNC at low concentration in the composites lacks its liquid crystal character due to the lyotropic mesogen of rod-like negative CNCs, which is easily impacted by external factors such as hydrogen bonding interactions with PVA. In ref 160, sodium sulfate was employed to produce nematic mesophases of CNCs during the clotting step of PVA/CNC fiber wet spin. In 2019, Kose et al.[34] and Mu and Gray[161] used glucose to improve the flexibility and pitch of CNC films, respectively. These latest ideas and novel exploitation methods can increase the mechanical characteristics of CNC inserted films/composites.

Mechanical grinding has been reported to produce a water-resistant flake vacuum[162] from structurally colored CNCs by utilizing desulfation and the intrinsic brittleness of CNC films; hence, CNC chiral tactoids are employed as structurally colored pigments. Mechanical characteristics of films are dependent on the uniform distribution of CNC tactoids over the films; hence, postprocessing is essential to stabilize the structure for future use. Desulfation of the dry material, either by the application of vacuum[162] or heat to the protonated CNC form[163] or through immersion in a strong base, can inhibit the redispersion of CNC films upon immersion in water.

Self-assembly of rod-like CNC results in mechanically fragile and thermally unstable iridescent films. The authors demonstrate that a simple alkali treatment may improve the toughness and thermal endurance of vacuum-filtered CNC iridescent films.[164] CNC particles merged with one another after treatment, and subsequent treatment led to fusion between ordered layers; hence, greater stress transmission between "chiral tactoids" might be a reason for improved mechanical characteristics.

These orientation aberrations were previously described as a result of the fusing of two pure CNC "tactoids", which resulted in the twisted, dislocated, or folded periodic bands that are commonly found as defects in the liquid crystalline phase of CNCs.[73] Neighboring "tactoids" with differing helix orientations may mix in the CNC water suspension, but the helix will not become uniform. It would take a considerable amount of time to correct a flaw of this scale into a uniform helix orientation.[73] However, this is impossible because constant water evaporation soon locks the system into a glassy state, prohibiting any further helix or director rearrangement.[165]

After evaporation, CNC films are likewise inherently nonuniform. CNC films are nonuniform due to two factors. The first is that the helix axes in the dried film are orientated at an

angle to the surface due to the random arrangement of helix orientations and variable pitch length values throughout the film. During the drying process, the film generates numerous "tactoids" with a cholesteric and well-organized structure, which may be examined by SEM. The helix axis orientations of these "tactoids" are not always the same, and their diameters vary as well. When these "tactoids" are gradually mixed and deposited, they can form a layered chiral nematic phase structure. Moreover, after drying, the "tactoid" will be pressed vertically, producing further helix axis distortion. Coffee ring effects generated by macroscopic nonhomogeneity are the second factor. Therefore, the particles are pushed to the border of the screen. Due to the creation of an unequal distribution of chiral "tactoids", "coffee ring" effects cause the film to have distinct colors. Because evaporation is greater at the periphery than in the center, capillary movement from the interior to the outside brings suspended particles to the droplet's edge and deposits them in a ring formed at the edge, resulting in ring-shaped deposits. As a result, the middle layer is thinner than that of the edge, and the optical characteristics of the corresponding location differ. The entire action causes the film's optical characteristics to be nonuniform.

Film thickness and management are both feasible. The most fundamental way is to employ mechanical force to produce a film with uniform and controllable optical characteristics using vacuum-assisted self-assembly. This method was used by Deheer et al.[166] In 2014, Chen and others[167] did more study on this technique. The films' orientation and consistent structure were reported to be high. The random distribution of spiral directions produced vibrantly colored films.

It was not the same as the uniform color achieved by the most widely used evaporation-induced self-assembly approach. Cross-section SEM images[168] demonstrate a very good local chiral structure. Faster evaporation causes the pitch size to rise and perturbation in the film structure. Because the temperature, casting area, air velocity, and humidity all influence drying rate, the ability to monitor and change these factors is crucial. Because the necessity for delayed drying limits film scalability, other approaches for generating uniform films at appropriate time scales are required.

5.1. Rheomechanical Analysis. The foundation for techniques used in the industry or laboratories can be developed with the aid of rheology research. Diffusion, rheology, and sedimentation are examples of nonlinear collective features of colloidal suspensions, which are composed of spherical rod particles suspended in a Newtonian liquid. For instance, viscosity can vary significantly. To handle these superstructures, it is necessary to understand the flow behavior of CNCs; for example, 3D printing of these liquid crystals necessitates an understanding of their shear recovery after printing. In contrast to CNC suspension, the creation of liquid crystalline structured domains also affects the macroscopic flow characteristics of CNC suspensions. Examining the literature shows that the general flow behavior of CNC suspensions under shear has been studied as well as the effects of concentration, surface charge, sonication, and temperature on their viscosity.[169−172] After analyzing the flow parameters of CNC suspensions over a large range of concentrations, it is now possible to characterize the microstructural transition from isotropic to anisotropic chiral nematic;[79,169,171] so rheology in this manner has been used as a characterizing role. When the CNC concentration is increased, the suspensions undergo another transition from liquid crystal to gel.[170] The addition of NaCl electrolyte to CNC aqueous

suspensions has been shown to affect the microstructure of the suspensions as well as the critical concentrations of liquid crystal phase formation.[75,76] These microstructural changes can have an immediate impact on the rheological behavior of CNC suspensions.[173]

The influence of ionic strength on the rheology of the microstructure of CNC solution was investigated using optical microscopy and rheometry as a function of CNC concentration and NaCl concentration (0−15 mM).[96,171] CNC suspensions were found to be isotropic at low concentrations and produce chiral nematic liquid crystalline structures and gels above the first critical concentration. Raising the ionic strength of the system to 5 mM NaCl concentration reduces the electroviscous effects and thus the viscosity of isotropic CNC suspensions; however, for biphasic samples containing chiral nematic liquid crystal domains, increasing the ionic strength to 5 mM NaCl concentration reduces the size of the chiral nematic domains and thus increases the sample viscosity.

At high shear rates, however, where all the ordered domains are shattered, the viscosity drops with NaCl addition. The addition of NaCl up to 5 mM weakens the gel structure and reduces viscosity. Further NaCl addition (10 and 15 mM NaCl concentration) causes considerable aggregation and destabilization of the CNC suspensions.[96] Increasing the ionic strength up to 5 mM NaCl in biphasic samples decreases the size of chiral nematic domains, resulting in an increase in viscosity at low shear rates. A thorough investigation of CNC chiral nematic structures would be fascinating to see the influence of changes in twisting angle and pitch length and how these manifest in rheology. Other suspensions[174] showed that while the loss modulus remained relatively unchanged in discotic mesogens finer textures resulted in a much lower storage modulus; following this trend, coarsening of the microstructure during textural relaxation increased storage moduli. As a result, the viscous component of the discotic mesophase pitch was found to be unaffected by the microstructure, whereas the elastic modulus was reported to be sensitive to layer-plane orientation and texture size.

Xu and Gao measured the rheological properties of aqueous GO liquid crystal dispersion to obtain information on liquid structural information, which revealed a reduction in shear viscosity at the I−N phase transition as a result of LC alignment along the flow direction.[175] Yang et al.[176] later confirmed strong shear thinning behavior and relevant shear alignment for a broad concentration of graphene liquid crystal dispersion. A complementary analysis of order parameters improves the understanding of anisotropic colloids' rheological behavior. Song et al. reported a quantitative analysis on the flow-induced alignment of suspension, in which the velocity profile and order parameter of flowing GO dispersion in a cylindrical tube were determined using optical birefringence and dichroism.[177] A decrease in viscosity was also observed near a critical volume fraction of $\Phi = 0.33\%$, indicative of a biphasic transition. Measurements of the storage and loss moduli confirmed the LC and gel-like phases, where well-defined elastic shear modulus and yield stress increased with GO volume fraction following the power law. Wallace et al.[178,179] also attempted to establish a link between rheological properties and other parameters governing LC formation in GO suspension; in their study, an I−N transition is explained solely based on the competition between orientational and position entropy in the theoretical framework of Onsager's theory, which was originally developed for rigid rods. GO, on the other hand, is a mechanically flexible mesogen,
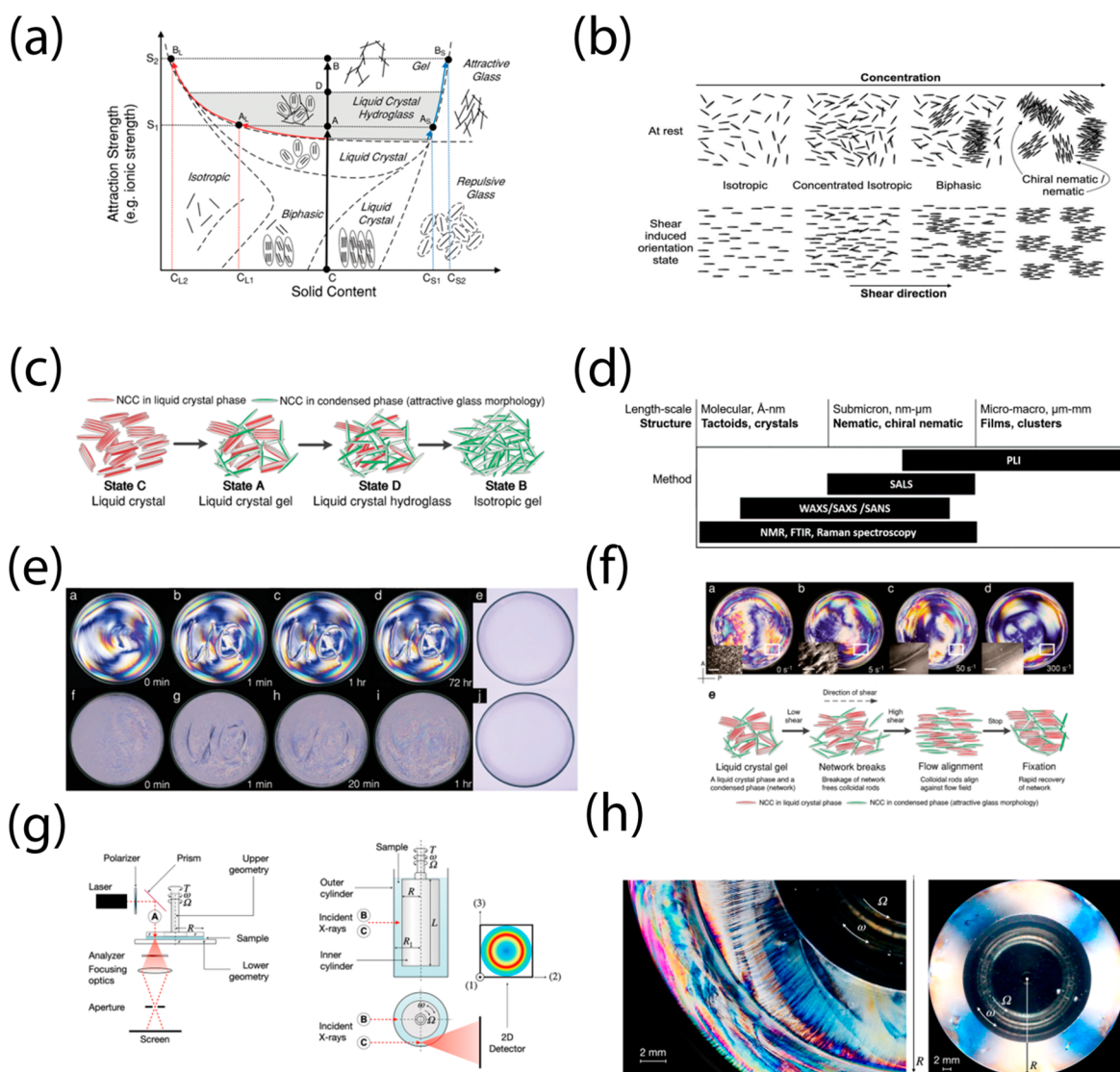
Figure 4. Rheological behavior of the liquid crystalline state of CNC in suspension and gel form. (a) Detailed phase diagram showing the isotropic, biphasic, liquid crystal, repellent glass, liquid crystal, and hydroglass states of CNC as a function of interaction strength and solid content of CNC. Salt causes liquid crystalline layers to melt gradually. The line linking C-A-D-B depicts the gradual transition of the system from a liquid crystalline state to a gel state, and the red stacks represent LCs. Adapted with permission from ref 182. Copyright 2019. American Chemical Society. (b) CNC self-assembly with rising concentration in a suspended at rest suspension (top row) and matching assembly in shear (bottom row). Adapted with permission from ref 182. Copyright 2019. American Chemical Society. (c) Hydroglass behavior that is shear-dependent: when shear is increased, the proportion of liquid crystals in the biphasic mixture of crystals and individual particles grows. (d) Displays the length scale of observations, the associated CNC structures, and suggested rheological methods for investigating these structures. (e) Visual representation of the viscoelastic properties of hydroglass and LCs, which are unable to disperse strain brought about by converting "UQ" into a liquid crystalline state. Due to the sluggish dynamics of the mixing of LCs and isotropic particles, as previously discussed in the glass-jammed and gel state, the amount of dissipation reduces as the attraction intensity increases (see Figure 2b). Adapted with permission from ref 182. Copyright 2019. American Chemical Society. (f) Linked behavior of hydroglass is illustrated schematically and graphically, and more liquid crystals develop because of orientation. (g) Rheo-SAXS/WAXS/SANS setups and rheo-SALS generic representations. Specifics like differences in SAXS and WAXS detector locations and beam stops have been left out. There are several possible building alternatives depending on the design. Adapted with permission from ref 182. Copyright 2019. American Chemical Society. (h) Display of CNC birefringence patterns using a custom transmission mode arrangement similar to those described elsewhere. Adapted with permission from ref 182. Copyright 2019. American Chemical Society.

as opposed to hard rigid rods; therefore, I−N transition might not obey Onsager's theory completely due to waviness and flexibility. Studies on GO suspension are easily extendable to CNCs; however, differences between the geometry of the two should be taken into account.

Wallace et al.[178,179] also claimed that because all GO sheets are parallel to the director during the nematic phase there should be a considerable loss in configurational entropy, and the influence of solvent molecules should also play a role. They attempted to optimize the system by concentrating on the rheological features of the GO dispersion range at fixed concentrations. The huge GO liquid crystals exhibited full nematic behavior as well as non-Newtonian flow curves with yield values, indicating that they are appropriate for wet spinning. Small GO sheets, on the other hand, acted almost exactly like Newtonian liquids, with no yield and no spinnability. GO dispersion of intermediate size produced biphasic regions with low yield values suitable for short-range fiber spinning.

Wallace et al. reported the viscoelastic properties of GO dispersion as a function of concentration while keeping the size of GO sheets constant at ultralarge dimensions (aspect ratio ~450 000).[178] Yield stress appears at ultralow critical concentrations ($\Phi \approx 2.2 \times 10^{-4}$), much lower than the theoretically predicted value for colloidal dispersions ($\Phi \approx 0.5$), which represents one of the lowest processing concentrations reported for 2D colloids.

Elastic and viscous moduli of GO dispersion were also measured as a function of concentration and frequency. At GO concentrations (<0.25 mg/mL) G'' was larger than G', indicating a viscoelastic liquid-like behavior suitable for electrospray or spray coating of GO dispersions. In the concentration range of 0.25−0.75 mg/mL, biphasic behavior dominated, with the storage modulus becoming larger than the loss modulus at large time scales, suggesting crowding in the system. Meanwhile, the intermediate time scales showed that G'' was larger than G', i.e., a yield that is suitable for inkjet printing. The distance between G' and G'' became larger at a concentration of 0.75−2.5 mg/mL where a full nematic phase was formed. In this condition, the crossover of G' and G'' shifted to a higher frequency typical of soft glassy materials that are the best fitting for wet spinning applications.[180]

Shifting focus from GO suspension to CNC suspension displays that these materials share similarities. Figure 4a displays an extensive phase diagram exhibiting isotropic, biphasic, liquid crystal, repulsive glass, liquid crystal, and hydroglass states of CNCs as a function of interaction intensity and solid content of CNC. Salt gradually melts liquid crystalline phases; the red stacks depict LCs, and adding salt progressively causes the system to move from a liquid crystalline state to a gel state, as shown by the line connecting C-A-D-B. The phase diagram shown here is more extensive than the diagram shown in the review published recently;[102] therefore, following this phase diagram is recommended.

Figure 4b exhibits CNC self-assembly suspended at rest, suspension with increasing concentration (top row), and matching assembly in shear (bottom row). This graph depicts the state of rod suspension in shear flow. Figure 4c shows a schematic representation of what happens when salt is added to the chiral nematic structure of CNCs; as shown, the addition of salt gradually leads to partial melting of the LC phase. Figure 4d attempts to demonstrate which techniques are useful for analyzing the scale of the LC of CNC, ranging from POM to SALS, SAXS, and Raman microscopy.

Figure 4e depicts the behavior of a hydroglass phase on CNC when illuminated with cross-polarized light. The top row shows a cross-polarized image of CNC liquid crystal hydroglass and liquid crystal suspensions of CNC with 35 mM NaCl at a concentration of 5%, while the bottom row shows a liquid crystal suspension at 7%. Sliding a pipet across the samples produced the letters "UQ". Flow patterns within liquid crystal hydroglass are durable within a liquid crystal suspension, revealing the suspension's ability to maintain structural alignment. This study demonstrates that by varying the ionic strength it is possible to create a structure with both liquid crystalline and isotropic phases.

Figure 4f analyzes liquid crystal formation and its impact on rheological properties. The ability of soft glassy materials to age with time is a common feature; to achieve equilibrium, the microstructure slowly evolves with time, resulting in time-dependent rheological properties, and the system is said to "age". Colloidal suspensions exhibit glassy behavior above a certain volume fraction where particle motion is sluggish despite still being structurally a liquid.[181] Figure 4g and h illustrates coupled devices used to analyze the LC behavior of CNC under flow; Rheo-SALS and rheo-SAXS/WAXS/SANS were coupled with rheometers to infer structural information.

At low shear network failures, the material's reaction to shear was then assessed, with greater orientation leading to the creation of a more liquid crystalline phase. In a phase transition for CNCs as a function of the concentration and salt that was based on rheological and structural study, multiple solid phases, including gel, repulsive glass, and attracting glass, were rheologically separated.[102] On each side of the liquid−solid crossover that happens as salt levels rise, the scientists found two more zones on the phase diagram: an anisotropic biphasic liquid crystal phase and a reentrant liquid crystal phase. The CNC suspension changes from isotropic to re-entrant LC, biphasic LC, and eventually isotropic gel as the ionic strength rises.

Rheological studies may be expanded to include situations in which CNC is combined with other previously studied ingredients such as PEG, glycerol, gold nanorods, or even gum Arabic. In a thorough rheological investigation of the behavior of CNCs in freshwater, Buffa et al.[183] concentrated on the salient features of rod-like suspensions that aligned under flow and can display liquid crystal behavior at rest, at least in a range of concentrations. Various surface modifications on the CNC were carried out by using TEMPO (TCNC), chloro(dodecyl)-dimethyl silane (DCNC), and trimethylsilyl propyl methacrylate (MCNC), also known as TCNC, DCNC, and MCNC. The impact of adding a dispersion agent (gum Arabic (GA)) to the suspension was examined. The stable suspensions created by the addition of CNC, TCNC, and GA had a concentration range where isotropic and anisotropic (self-organized) phases coexisted in balance. While exhibiting a similar sort of rheological behavior to the other nanocrystal suspensions, the two silanized CNCs' aqueous suspensions, on the other hand, only displayed flow-induced ordering and had substantial quantitative differences. After a few hours of relaxation, these latter suspensions precipitated since they were not stable. For all the nanocrystalline solutions made at different concentrations, rheological experiments were performed using steady shearing, dynamic oscillations, and steady shear start-up. The observed variations resulted from either modification to the crystals' surfaces or inclusion of a dispersion agent. A sustained periodic oscillation of viscosity was observed during in the start-up of steady shear testing. The times of the oscillations were identified and connected to the various types of crystals under consideration.

Additional rheometric information, other than shear flow, can be utilized to extrapolate more structural details about rod suspension in glass or gel states. A note should be made of the finding of a negative initial normal stress differential (N1) in the biphasic suspension. When elongated nanoparticles or rods are aligned with the flow, they travel in a way that causes N1 to encounter a minimum that can be negative in value.[184] A similar behavior is observed in polymer melts and solutions.[185] An aqueous solution of the generated cellulose polymer hydroxypropyl cellulose has also been shown to have this response.[186,187]

Biphasic LC phases do not fall within the Cox−Merz rule because the suspension has a time-dependent structure. The shearing viscosity vs shear rate (s^{-1}) and the complex viscosity vs angular frequency ($rad \cdot s^{-1}$) coincide when the Cox−Merz rule is followed by a material. It is not always acceptable to have this

regulation followed, particularly in the event of CNC suspensions.[170,183] This has been observed for microcrystalline cellulose in an ionic liquid media solution of 1-allyl-3-methylimidazolium chloride,[188] in addition to all of the aforementioned features. Furthermore, testing for liquid crystals using small-amplitude sinusoidal oscillations cannot produce concentration−master curves. For these biphasic CNC suspensins,[170] the method of creating a master curve by frequency shifting the curves of dynamic characteristics acquired at a given concentration, such as storage and loss moduli, does not provide clean curves.

6. APPLICATIONS

6.1. Responsive Materials. Building stimuli-responsive (may rely on moisture, heat, phase separation, etc.) materials that can match the complexity of biological systems offers great potential when the cholesteric helix is controlled. Low-cost biodegradable optical sensors may be made because the underlying nanostructure determines the reflected color structural response to an external stimulus. The use of CNC-based sensors has been documented for detecting humidity,[158,189] solvent,[190] and measuring pressure.[190] For instance, CNC-based films are advantageous due to their inherent sensitivity to water. Due to their poor water resistance, they shed their prized iridescent tint even after being slightly swollen by water, which restricts their employment in environments with typical humidity levels.[191] However, since the CNC chiral structure is so sensitive to dampness, it makes a great humidity sensor. Recently, research on the coassembly of CNC with oxidized starch and tannic acid to increase CNC's solvatochromism was conducted in contrast to changes in moisture content. The composite film retained its structural stability and brilliant structural color after being soaked in water for 24 h. In addition, mechanical properties[192] were improved thanks to cross-links created by tannic acid. This study also shows that tannic acid or starch treatment of CNC does not interfere with the self-assembly procedure. With the use of the knowledge presented here, it may be possible to adjust the chiral structure of CNC's level of sensitivity, meaning that the degree of assembly with other substances like starch or tannic acid would affect how sensitive the chirality is to humidity.

Guo et al.[193] showed how nematic LC phases of GO may be shaped into distinct supramolecular architectures by the use of surface attachment, complex fluid flow, and microconfinements. A characteristic folding and unfolding process that is sensitive to hydration may be seen in GO LCs. Surface-aligned GO phases were seen during the drying−rehydration sensitive unfolding and expanding transition. Due to the buckling instability caused by surface tension, folded structures store electric energy when they are dry. As a result, changes in humidity can also reshape films; during this process, the interfacial interaction frictional forces are lowered after rehydration, liberating the energy while expanding. This unique GO behavior opens a wide range of opportunities for stimuli-responsive materials, cutting-edge nano- and microelectromechanical devices, dynamic space filling and sealing applications, and more. The comparability of the two systems allows for a replication of this work for CNCs. Eventually, a humidity-gated photoactivation synthetic nocturnal blossom that closes in daytime settings when humidity is low or light levels are high and opens in the dark when humidity is high was developed.[194] This artificial flower was inspired by nature. This makes it possible to use LCs for soft robotics and home decoration applications.

He et al.[195] developed CNC nanocomposites that reacted to mechanical forces and moisture by utilizing glycerol as a plasticizer. The film's chiral structure[195] can be changed to alter the structural color. When subjected to relative humidity levels ranging from 16 to 98%, the film showed reversible color change. The film may also quantify compression pressure by altering the color of its iridescence. Inducing gas-detecting characteristics on CNCs, CNC-based films can also exhibit a dual reaction to moisture and formaldehyde gas[196] with reversible structural color change. When paired to a simple formaldehyde response,[196] the color modification caused by formaldehyde can change from being imperceptible to noticeable when the film is subjected to a humid environment.

CNC's chiral/optical properties can also be made tunable concerning certain solvents. The researchers developed a new technique for creating mesoporous CNC films based on this. Giese and colleagues[190] used an alkaline solution to treat a composite of CNCs and a urea-formaldehyde (UF) resin to create mesoporous photonic cellulose (MPC) film that could change structural color in the visible-light range quickly and reversibly in a polar solvent. They reported that the composite material's absorption peak wavelength in 100% ethanol was 430 nm but that it was 840 nm in pure water. The color will "shift" to red as the amount of water increases. The mesoporous structure was created during supercritical drying, and the decreased crystallinity (relative to the crystallinity of the initial CNC films) gave rise to the synthetic cellulose films' notable flexibility properties. Additionally, because of its fast and reversible color change upon swelling, this MPC film is especially suited for pressure sensing. These novel active highly porous cotton materials have potential applications in tissue engineering, chiral separation, biosensing, and functional membranes.

PEG-induced "depletion attraction" has been allowed in a number of systems, including DNA and lyotropic LCs.[197] Changing the molecular weight of PEG can change the optical characteristics of CNCs with chiral nematic structures.[103] Because pure CNC films are brittle, several water-soluble polymers have been added to increase film flexibility and mechanical strength, including poly(vinyl alcohol),[198] PEG, and polyurethane.[199] The color of the film may be modified by changing the pitch size of these water-soluble polymers. As a result, adding PEG has two effects: one, it raises the mechanical characteristics of the CNC film, and second, it alters the pitch size due to depletion forces.

Iridescent colors may be changed from red to blue by depletion by varying the proportion of polymer; however, mechanical qualities can also change with polymer addition. The concomitant rise in mechanical properties opens up a wide range of applications, such as humidity sensors, force sensors,[34] and anticounterfeiting papers,[200] to these structures. To offer some data, the reflectance spectra of pure CNC films exhibit a peak at 242 nm that grows to 361 nm when the PEG weight fraction increases up to 30 wt %; moreover, when the PEG concentration surpasses 25 wt %, the reflectance band becomes significantly broader. Tuning reflection spectra may produce items such as inks,[201,103] home décor, and so on. The half-pitch diameter increases from 103 to 143 nm when the PEG weight fraction increases from 10% to 20%. The pitch size can also change by modifying the molecular weight of the nonadsorbing polymer; similar behavior was demonstrated in ref 103.

Despite the fact that the first investigations on limited Brownian diffusion were undertaken many years ago,[202] this issue has lately been studied.[203] Understanding how a sphere
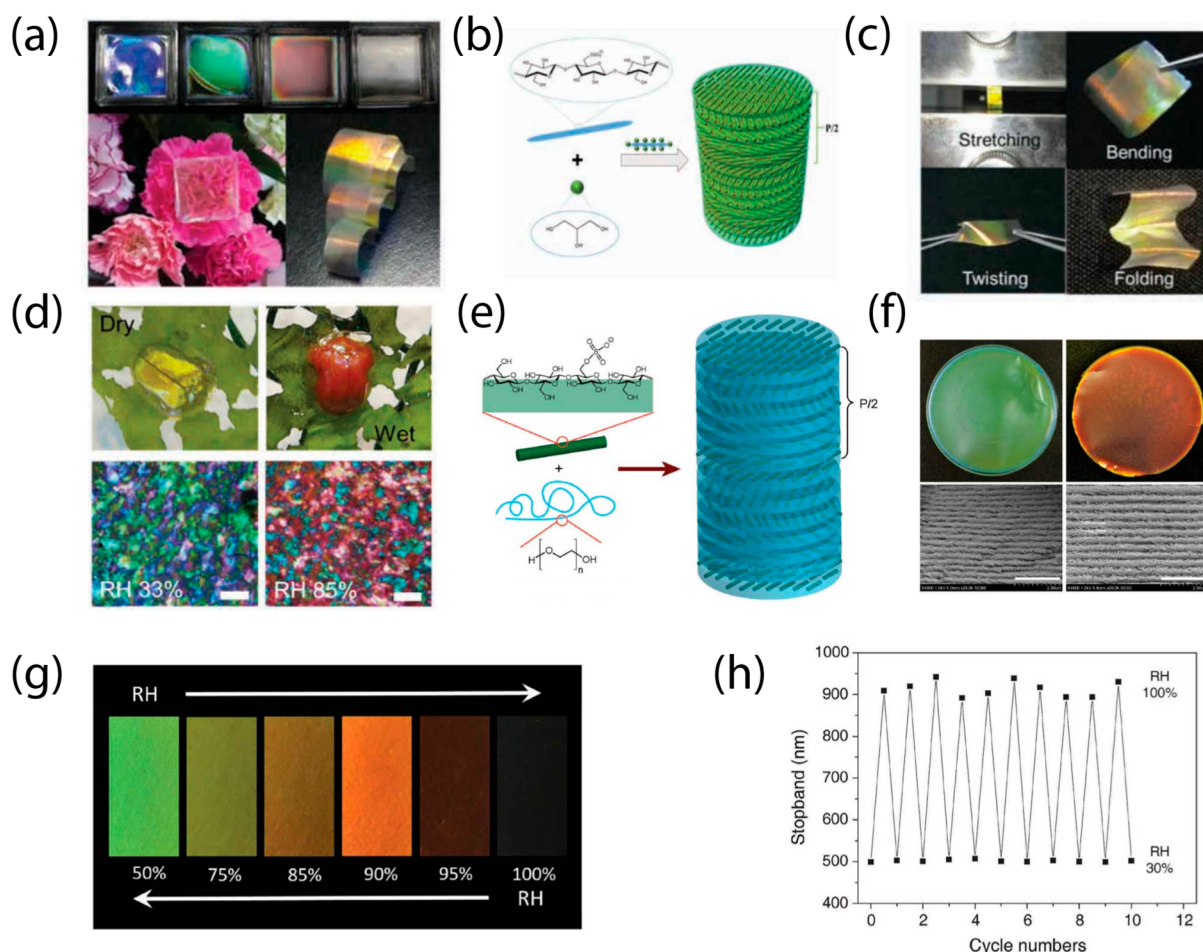
Figure 5. External influences cause iridescent changes. (a) Digital images of pure CNC and CNC/glycerol composite films were obtained under white light. The top films, which are pure CNC, CNC/Gly20, CNC/Gly40, and CNC/Gly50 composite films, are blue, green, red, and colorless. A flower is covered with the CNC/Gly20 film, which is then folded into an iridescent bridge at the base. Adapted with permission from ref 201. Copyright 2018. Royal Society of Chemistry. (b) Schematic representation of the method for assembling cellulose nanocrystals and glycerol into chiral nematic structures. The pitch of a half-helical spiral is P/2. Adapted with permission from ref 201. Copyright 2018. Royal Society of Chemistry. (c) A variety of conditions led to deformation in the CNC/Gly30 composite film. Patterns of X-ray diffraction for pure CNC film and for CNC/Gly composite films with various glycerol contents. Adapted with permission from ref 201. Copyright 2018. Royal Society of Chemistry. (d) The color of the beetle changes in a dry and wet habitat. Adapted with permission from ref 210. Copyright 2007. American Physical Society. POM images of the CNC/Gly20 film at different relative humidity (RH) levels; these dramatic variations resemble beetle growth (scale bar: 500 mm). Adapted with permission from ref 201. Copyright 2018. Royal Society of Chemistry. (e) The creation of CNC/PEG composites with chiral nematic structure because of CNC self-ordering is depicted schematically (P/2 stands for half-helical pitch) (what effect PEG had on pitch length). UV and visible reflectance maxima in the transmission spectra of CNC and CNC/PEG composite films occur at 30% relative humidity. The chiral nematic structure's pitch size in the solid films may be controlled by varying the CNC and PEG mix, creating composite films with an adjustable photonic bandgap. Adapted with permission from ref 123. Copyright 2017. Wiley-VCH. (f) Visual portrayal of films as relative humidity changes. Adapted with permission from ref 123. Copyright 2017. Wiley-VCH. (g) The color shift of composite films was studied in response to gradually increasing and decreasing RH between 30% and 100%. Copyright 2017. Wiley-VCH. Adapted with permission from ref 123. (h) Chiral nematic structure resiliency to varied cycles and relative humidity values. Adapted with permission from ref 123. Copyright 2017. Wiley-VCH.

moves under confinement is crucial because it may be used to depict particles moving in porous media or near fluid–solid boundaries, macromolecules diffusing in membranes, or cells interacting with surfaces.[204] Aside from the influence of the wall on particle Brownian motion, it has been observed that hydrodynamic coupling of two colloidal spheres over a barrier alters the attractive interaction of spheres.[205] LCs are a useful structure to explore for Brownian diffusion since they are easily produced using lyotropic CNC suspension. The literature[206] has only seen CNC LC rearrangement and has not offered any information on whether confinement can influence transition points by shifting the point of transition to lower or higher particle concentrations.

The easiest form of LC under confinement is the evaporation of a tiny volume of iridescent solution on a Petri plate, which results in thin sheets. Brilliant structural colors may be generated even when the thickness of such films is just an order of magnitude larger than the pitch length.[207] A planar orientation of the cholesteric nanostructure is easily formed in such thin-film confinement,[208] even under quick-drying circumstances where disclinations in the cholesteric order are supposed to be kinetically confined. The evaporation of a tiny volume of luminous liquid on a Petri plate creates thin films, which is the most basic example of LC under confinement. The discontinuous pitch shift caused by these disclinations is critical in extremely thin films (approximately 1−2 nm) and can result in a

mosaic of different colors.[91] Some accounts claim that confinement leads the bulk isotropic-to-nematic transition to become a continuous ordering from an isotropic to a nematic phase; moreover, confinement obscures translational order in smectic crystals.[209]

A range of CNC-based nanocomposite materials were developed and tested to reproduce the cholesteric colorful creatures observed in nature. CNC/Gly films displayed reversible reflection colors with altering relative humidity due to glycerol's strong water absorption ability. Figure 5a shows a white-light picture; digital photographs of pure CNC and CNC/glycerol (Gly) composite films were also taken concurrently. The top blue, green, red, and colorless films are pure CNC, CNC/Gly20, CNC/Gly40, and CNC/Gly50 composite films. The CNC/Gly20 film is put on a flower and folded at the bottom to form an iridescent bridge.[201] These photos show color variations caused by the addition of glycerol to CNC. Figure 5b depicts a schematic of the glycerol assembly. The produced films are also highly robust due to their ability to be folded, twisted, reinforced, and compressed; they may be employed for a wide range of purposes and characteristics (see Figure 5c). At changing degrees of relative humidity, the produced composite film displays comparable hue variations to how the color of a beetle varies in a dry and wet environment (see Figure 5d). In summary, the researchers created humidity-responsive films, photonic inks, and iridescent coatings using a range of multifunction structure nanocomposites with adjustable and tunable colors. By varying the glycerol content of the CNC composite films, the colors of the reflections can be altered as shown in a series of figures displayed in Figure 5a–d.

Figure 5e shows a sequence of images for the CNC/PEG film with a ratio of 80/20 exposed to cyclic humidity conditions. The dry film was subjected to humid air at relative humidity (RH) values ranging from 50% to 100%, and structural color changes in the visible spectrum were observed. The sample had a comparable green color at 30% and 50% RH. As the RH increased from 50% to 100%, the film transformed from green to olive, brown, orange, dark-red, and clear, which is consistent with the UV reflectivity. The expansion of the multilayer structure due to penetration of water leads the structural color to shift to red at high humidity. When the RH was reduced, the change in periodic multilayer structure was reversed. After the RH was gradually reduced from 100% to 50%, the transparent film returned to dark red, orange, brown, olive, and green. Figure 5e depicts the manufacturing of CNC/PEG composites with chiral nematic structure caused by CNC self-ordering; additionally, chiral moieties were characterized by analyzing transmission and reflection spectra of CNC and CNC/PEG films with UV and visible reflectance at 30% relative humidity. The results clearly reveal that the interaction with light of CNC and PEG is adjustable; i.e., PEG addition modulates the pitch length and chirality of CNC in solid films. Furthermore, the color shift of composite film was evaluated visually in response to tuning (increasing/decreasing) humidity values ranging from 30 to 100%; hue shifts with relative humidity are striking. Figure 5h displays the stop band as a function of multiple wetting and dewetting cycles. Figure 5h depicts that although the peak location varied slightly the plot remained consistent (position of the peaks), and the shift in peak position was reproducible and reversible, indicating the composite film's excellent stability and reversibility.

Suspension may also produce a variety of iridescent colors, which are tunable due to uneven film development on various surfaces. The effect of CNC cholesteric phase growth as a function of the substrate on which the solution dried out was examined in ref 211. When CNC dispersion was dropped on the substrates, the impact of the substrate on the fading out of CNC suspension and its liquid crystal formation behavior was observed. On stainless steel (SS) and glass, CNCs exhibited initial contact angles of 57.32 and 37.83, respectively.

The cholesteric layer self-assembled from the droplet's bottom center and diffused to the hydrophilic glass substrates' edges.[212] As a result of the edge-center ordered drying technique,[135] the iridescent coating films formed on PS, SS, glass, Cu–Zn alloy, and Cu–Ni alloy display characteristic "coffee rings". The conclusions of this study apply to spray coating on a variety of substrates; research reports on whether iridescent color spontaneously appears on examined surfaces. As a stimulus-response material, developed iridescence can indicate the nature of the surface. Thermotropic LCs are interesting guests to be included in chiral systems because they display large variations in indices of refraction and molecular alignment induced by temperature changes, providing a thermal switch to regulate reflection in chiral nematic highly porous organo-silica films. In 2013, researchers used the thermotropic liquid crystal 4-cyano-4′-octyl phenyl (8CB)[213] to penetrate octyl-functionalized chiral nematic organo-silica films. The films are very iridescent at room temperature; when heated, they rapidly change to colorless at the nematic to isotropic transition point for 8CB at 40 °C.

The absence of the reflection signal in the UV–vis spectra for the LC-loaded films clearly demonstrates the changes in optical properties. In a study, poly(N,N-dimethylamino ethyl methacrylate) was bonded on CNC, and the resultant lyotropic fingerprint texture varied with temperature.[214] As a result, future studies should focus on this feature of CNC chiral structure as well.

SEM was used to examine CNC film cross sections, and optical microscopy was used to examine CNC photonic film pitch; the findings revealed a low-temperature dependence.[215] The cholesteric stripe's bright and dark margins were not equal, and their difference changed significantly depending on temperature and nematic phase type. The transition between calamitic cholesteric (Ch_C) and discotic cholesteric (Ch_D) and one biaxial cholesteric (Ch_B) was studied. Ch_C–Ch_D and Ch_B–Ch_C transitions were visualized using optical microscopy.[216] The alteration of photonic material optical properties is an important aim in the development of reflective screens, filters, and detectors. The optical properties of optical substances might be adjusted by treating both their periodic and refractive index difference. Guests placed within the channels of a chiral nematic mesoporous host might allow for stimuli-induced changes in refractive index and hence dynamic modification of the optical properties of the composite. Therefore, CNC chiral structures may be made temperature change programmable.[217]

6.2. Energy Storage Applications. Nanocellulose is gaining popularity because of its renewable and carbon-neutral nature, remarkable biocompatibility, tailorable surface chemistry, and unmatched optical and mechanical properties.[1] The purpose of this study is to provide an up-to-date appraisal of recent nanomaterial advances and their potential applications in soft robotics, energy storage, and medicinal science. The introduction of hierarchy and chirality into structures is of great interest because it has the potential to provide novel optical and electrical characteristics owing to the synergistic impact of helical and anisotropic structures. To employ CNCs for energy

storage applications, conductivity must be added to them; this may be accomplished by mixing CNCs with a conductive filler or coating CNCs with a conductive polymer. For example, for potential energy storage applications, CNC can be coupled with such a 2D graphene oxide nanostructure and loaded with active SnO_2. The resultant SnO_2/CNC/reduced GO (SnO_2/CNC/ reduced graphene oxide (rGO)) composite has a tensile strength of 100 MPa and may be manufactured as a film, fiber, or fabric.[218]

The free-standing (SnO_2/CNC/rGO) electrodes demonstrate much improved energy storage capability at a current density of 500 mA/g,[218] with a reversible capacity of 500 mAh/g maintained for 1500 cycles in the film and 800 mAh/g maintained for 150 cycles in the textile. Germania was also integrated into chiral nematic CNCs using the sol–gel process in another work. The approach conserved the order of the original chiral nematic CNC aerogels, resulting in hybrid aerogels with a high concentration of randomly dispersed GeO_2 nanoparticles and specific areas as large as 705 m^2/g. The carbonization of the composite material produced a highly ordered material with no compression collapse and good form restoration after release. The combination of the electrolytic double-layer capacitance of the carbon-containing skeleton and the pseudocapacitive contribution of the GeO_2 nanoparticles resulted in materials with a maximum C_p of 113 F/g and high capacitance retention.[219] Likewise, the author of ref 220 polymerizes pyrrole in situ onto modified chiral nematic CNC sheets by covering them with a conductive polymer. TEMPO-oxidation, acetylation, desulfation, and catonization had no effect on the chiral structures. Because they are simple to make, these new materials offer tempting alternatives for environmentally friendly sensors and energy storage devices. It should be noted that the chiral structure was unaffected by TEMPO oxidation, acetylation, desulfation, or cationization.

Artificial chiral material produced employing nanomicrosized matrices has benefitted chemical synthesis, chiral sensing, chiral catalysis,[221] and meta-material-based enhanced optical devices. Hard template techniques and soft template methods are the two most used methodologies for manufacturing chiral substances. These methods may be utilized to develop novel nanostructured materials with chiral characteristics. (i) When producing chiral materials, hard template techniques are widely used as a mesoporous host to transfer their nanostructure to other materials. (ii) Soft template method: material is generated by selectively removing the host template. To prepare the template, molecular evaporation, rapid self-assembly, or supramolecular aggregation is used. Soft template preparation is more flexible than hard template preparation for nanomesoporous materials.

Pattern generation from nanocolloidal LCs in constrained geometry, also known as templates, can be utilized as a template for nanoparticle organization. Three-dimensional confinement of cholesteric liquid crystal was explored in ref 222 under two-dimensional confinement. The phase-separated cholesteric shell was constructed using concentric CNC pseudo layers with a helicoidal axis perpendicular to the inner surface of the capillary walls and an isotropic core thread running parallel to the capillary's long axis. As the degree of confinement rose, the shape of the LCs was altered, indicating that the generated core–shell LCs might be employed in optical waveguides. According to the scientists, POM was used to examine the structure over time, and after 6 h, a well-defined isotropic core was produced, which did not relax until 168 h had passed. This suggests that isotropic

and cholesteric CNC rearrangement takes time.[222] The pattern generated in this study can be coupled as well to position the nanoparticle or polymer attached to CNC liquid crystal in parallel to the long axis of the CNC fiber, therefore unlocking further potential.

In ref 223, mesoporous titanium dioxide (TiO_2x) with the chiral nematic structure of a core–shell nanorod was characterized via templating once again. Carbonized TiO_2/ CNC helical materials are created by chirally transferring TiO_2 nanoparticles onto gelatin-functionalized CNCs and then calcinating CNCs to recover TiO_2 chiral copies after the cellulose is removed. The black TiO_2x is a semiconducting mesoporous structure composed of chiral nematic crystalline–amorphous TiO_2 core–shell nanorods. This research has immediate application in industry as the anode electrodes of lithium-ion batteries are made up of chiral black TiO_2x nanoparticles supported by mesoporous nanocarbon networks. Beyond the current efforts, these black TiO_2x materials and composites may be useful in the fields of energy storage and catalysis (for instance carbon monoxide oxidation).[224] Evaporation-induced self-assembly of CNC with silica precursors, according to MacLachlan et al.,[225] can result in composite films containing chiral nematic structures. After pyrolyzing and etching the CNCs, freestanding sheets of chiral nematic mesoporous carbon are formed. In a symmetrical capacitor with H_2SO_4 as the electrolyte, mesoporous carbon sheets display near-ideal capacitor behavior, with a specific capacitance of 170 F g^{-1} at 230 mA·g^{-1}. Figure 6 depicts a template procedure in which a CNC was calcined to form a completely silica aerogel; the pitch width and orientations were also recorded before and after calcination.[226]
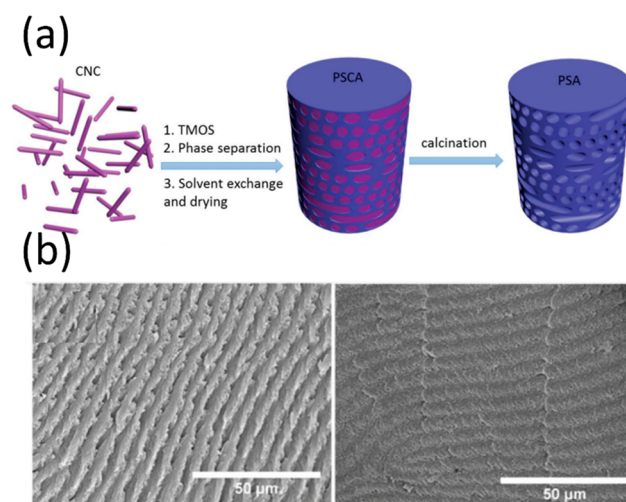

Figure 6. Templating method in CNC cholesteric structure. (a) Diagram showing how silica/cellulose aerogel and silica-only periodic aerogel are made. (b) Cross-section SEM images of periodic cellulose/ silica aerogels and periodic silica-only aerogels. Adapted with permission from ref 226. Copyright 2018. American Chemical Society.

Templating can also be utilized for diverse interactions with light. The templating process allows for more than merely transferring the helical structure to different materials. The inorganic duplicate's optical sensitivity might differ greatly from that of a dried CNC film. The refractive index of air and the single refractive index of the optically isotropic amorphous inorganic material are repeated discrete contrasts in a templated

amorphous inorganic film, whereas the latter has a continuously varying refractive index due to the rotation of the birefringent CNC rods. Therefore, the reflection may be switched on and off by filling the voids with an index matched fluid and drying the liquid. The switching may be very quick and reversible if the voids are filled with a thermotropic nematic, whose refractive index in the absence of a field matched that of the inorganic material. When an electric field is applied to a thermotropic nematic, the index matching is lost, and the film looks colored. Even though the initial dried CNC film is porous, such ON/OFF switching of photonic crystal characteristics is not achievable because a birefringent matrix material lacks an index matching fluid. In comparison to visible-light wavelengths, the thicknesses of the inorganic and air layers, as well as their sum (which forms the local optical period), are especially important for the colors produced. Prospective uses of transparent CNC-templated inorganic materials that have yet to be investigated include cholesteric-based mirrorless lasing.[227]

Finally, it should be highlighted that novel materials and technologies for energy storage should be researched, employing different types of nanocellulose and their combinations as building blocks, depending on the sizes, structures, and surface chemical performance of nanocellulose. This is because nanocellulose is manufactured from several sources utilizing a range of processes. By combining TEMPO-oxidized CNCs with transparent conductive materials, for example, optically transparent and flexible electrodes may be created. Chiral nematic mesoporous carbon electrodes may be made using sulfuric-acid-hydrolyzed CNC as a template as well. The investigation of novel materials and manufacturing techniques may lead to opportunities in a range of applications.

It is worth nothing that nanocellulose and its derivative substances have been widely employed in supercapacitors and lithium-ion batteries (LIBs); however, only a few investigations on their application in Li−S (lithium selenium) batteries and sodium-ion batteries have been published.[228] Furthermore, several novel energy storage devices, such as Mg (Al, Mn)-ion batteries, have received little attention. Nanocellulose and its derivatives may be easily tailored as a green material alternative for fast-growing energy storage devices since they are physically robust and have changeable structure and surface/interface chemistry.

6.3. Optical and Optoelectronic Applications.
Over the last few decades, technological improvements have frequently coincided with the creation of novel materials. Material scientists and engineers put forth a lot of effort to learn from nature's complex design principles while looking for inspiration.[229] For example, stimuli-responsive "smart" materials that alter form reversibly in reaction to external triggers open the way for soft robotics[230] and self-regulating devices[231] and bio-inspired hierarchical surfaces in wettability control and adhesion.[232]

The chiral structure of CNCs is used to template optical characteristics as well. A notable example of using CNC-embedded systems for optoelectronic applications is the production of crack-free, chiral nematic GeO$_2$/CNC composite films with tunable photonic properties from the controlled assembly of germanium(IV) alkoxides with "lyotropic" liquid-crystalline CNCs in a water/dimethylformamide (DMF) mixed solvent.[219] Photonic GeO$_2$/CNC composites may be transformed into semiconducting mesoporous GeO$_2$/C and Ge/C copies, freestanding chiral nematic films of amorphous GeO$_2$, and photonic GeO$_2$/CNC composites using different pyrolysis

conditions. These novel materials have applications in chiral separation, enantioselective adsorption, catalysis, sensing, optoelectronics, and lithium-ion batteries, among others. Furthermore, the unique, repeatable synthesis procedures outlined might be used to create a wide range of chiral nematically organized composites and porous materials.

As stated earlier, only left circularly polarized (LCP) light is reflected by CNC sheets, but this can change. Fernandes et al.[159] developed a novel photonic structure inspired by the cuticle of the beetle *Plusiotis resplendens*, in which chiral CNCs could reflect both LCP and RCP light. To construct this photonic structure, an anisotropic nematic liquid layer of 4-pentyl-cyano-4′-pentylbiphenyl was sandwiched into a microgap between two left-handed cholesteric nanocellulose domains with comparable pitches. The nematic layer is a half-wave retardation plate that converts RCP light to LCP light and vice versa. As a result, the RCP light may be efficiently reflected.[233] The transition from right- to left-handed could further be regulated by adjusting the temperature or applying electricity. At temperatures above the nematic-to-isotropic transition temperature, for example, all RCP light is transmitted (colorless reflection), whereas LCP light is still reflected, but at a longer wavelength, because the material refractive index decreases and the pitch of the cholesteric chiral phases increases.

Despite the fact that certain cellulose derivatives can produce chiral nematic LCs with both left- and right-handed structures,[234] CNC dispersions appear to invariably produce left-handed chiral nematic phases. CNCs can also incorporate photoluminescence. CNC's[235] chiral structure was created using a low molecular weight nematic liquid crystal, 4′-(hexyloxy)-4-biphenylcarbonitrile (HOBC). The resultant composite material combines the rich structural coloration of photonic cellulose with the thermal and conductive properties of nematic liquid crystal. Pitch length was constant after treatment with HOBC.[235] The twisted spindle feature in the edge view of the damaged film under SEM spun counterclockwise, demonstrating that the CNC formed left-handed helicoids. Photoluminescence was seen in nematic HOBC-LCs films.[236]

For broadband optical properties, variations in helical pitch length and helical axis orientations within film domains contributed to a subtly broader chiral reflection band, resulting in a broad band circular polarizer, i.e., the ability to reflect certain circularly polarized light while transmitting others. The work not only proposes a simple approach for producing a film with broadband reflection but also provides a model for examining the interactions between nanosized supramolecular aggregates and CNC assemblies (broadband reflection). These methods might be used to modify the optical characteristics of various chiral liquid crystal systems, which could be employed in optical filters, polarizers, and coatings.

Naturally derived CNC-based materials' flexibility, along with their biocompatibility, enables a wide range of uses, from low-cost decoration to more sophisticated objectives. Crushing CNC films into flakes of varied sizes produces edible structurally colored glitter or powder ideal for spray application in food coloring paints or cosmetics.[162] Aside from aesthetics, the ability to reflect just one polarization of light at a certain wavelength band is advantageous for anticounterfeiting.[30,200] Temperature, compression, swelling, magnetic field orientation, or other CNC-based depolarizing coatings, as well as optically active dopants such as upconverting brilliant dyes or nanoparticles, might be used to further diversify this property. Zhang and colleagues demonstrated that adding a fluorescent whitening

chemical to a CNC-based LC linear structure may enhance the spacing while keeping the iridescence features of the films at low concentrations.[200] Compared to the usual whole-film application, the effective techniques of proper grinding and different post-treatments produced films with a tiny platelet form and an average thickness of 25 μm.[162] These structural colors were maintained in fragment films, giving them an iridescent appearance and making them counterfeitable. Gan et al.[237] recently examined how a vertically built CNC and the associated film with an anticounterfeiting pattern could hide information under natural light when the CNC was shorter than 144 nm and disclose hidden information under UV radiation.

Optical diffusers provide soft light with a uniform spatial and directional intensity distribution. Because of their excellent scattering properties, optical diffusers have been widely used for uniform backlighting, scanning bar codes, computer screens and other monitors, luminance augmentation, efficiency, higher susceptibility in liquid crystal displays (LCDs),[238] light-emitting diodes (LEDs),[239] solar cells,[240] and photodetectors.[241] There is currently no documentation of research on the use of CNC chiral structures for optical diffusing.

7. CONCLUSION

This paper investigated the colloidal features of CNC and illustrated how to use them to develop value-added goods from CNC in the end. The capacity to modify the internal photonic crystal structure of cellulose-based LCs was established. By being low-cost, sustainable, and nontoxic, LCs created using CNCs compensate for the shortcomings of typical liquid crystal materials based on organic/inorganic components. Because of its easy availability of raw ingredients, simple manufacturing method, and low energy consumption, the innovative type of liquid crystal material has the potential for commercial large-scale use. Furthermore, the unique liquid crystal material exhibits chirality, making it an important study tool in the field. There are presently two methods for producing liquid crystal films from CNCs. One method for creating multifunctional composite materials is to include functional particles into CNC suspensions. The objective is to use the cellulose chiral nematic liquid crystal structure as a template for rapidly and correctly producing organic/inorganic liquid crystal materials with the same chirality. The second method is to employ them for photoresponsive materials; photoresponsive nanomaterials might enhance information processing devices, micromachines, and biosensors.

Because of the nanostructure's poor compatibility with the host medium, scalable production of such materials using mesostructured liquids such as LCs remains a difficulty. Photoswitchable chirality of plasmonic DNA-origami has already been established in cellulose nanofiber-based LCs.[242] The composite material inherits DNA-origami plasmonic nanostructure properties, allowing composite chirality to be erased and restored using UV light. Finally, any parameter that may affect the point of transition from isotropic to nematic or the chirality of CNCs can be used to tailor CNC chirality for a variety of applications. Because of the multiple uses those iridescent inks created by CNCs might give, it is possible that they will attract attention soon. There are other challenges as well that need proper investigation such as slip effects that affect the local organization of CNCs like other colloids[243] during a process adjacent to the walls. Investigation with this sort is largely unexplored in the literature.

■ AUTHOR INFORMATION

Corresponding Author

Aref Abbasi Moud − *Polymer and Color Engineering Department, AmirKabir University of Technology, Tehran, Tehran Province 1591634311, Iran;* ⊙ orcid.org/0000-0002-1396-287X; Email: aabbasim@ucalgary.ca

Complete contact information is available at:
https://pubs.acs.org/10.1021/acsomega.2c03311

■ REFERENCES

(1) Moud, A. A.; Kamkar, M.; Sanati-Nezhad, A.; Hejazi, S. H. Suspensions and hydrogels of cellulose nanocrystals (CNCs): characterization using microscopy and rheology. *Cellulose* **2022**, 1−33.

(2) Wang, L.; Urbas, A. M.; Li, Q. Nature-inspired emerging chiral liquid crystal nanostructures: from molecular self-assembly to DNA mesophase and nanocolloids. *Adv. Mater.* **2020**, *32* (41), 1801335.

(3) Kumar, J.; Eraña, H.; López-Martínez, E.; Claes, N.; Martín, V. F.; Solís, D. M.; Bals, S.; Cortajarena, A. L.; Castilla, J.; Liz-Marzán, L. M. Detection of amyloid fibrils in Parkinson's disease using plasmonic chirality. *Proc. Natl. Acad. Sci. U. S. A.* **2018**, *115* (13), 3225−3230.

(4) Zhou, C.; Duan, X.; Liu, N. DNA-nanotechnology-enabled chiral plasmonics: from static to dynamic. *Acc. Chem. Res.* **2017**, *50* (12), 2906−2914.

(5) Fraden, S.; Maret, G.; Caspar, D.; Meyer, R. B. Isotropic-nematic phase transition and angular correlations in isotropic suspensions of tobacco mosaic virus. *Phys. rev. lett.* **1989**, *63* (19), 2068.

(6) Blackmond, D. G. The origin of biological homochirality. *Cold Spring Harb. perspect. Biology* **2010**, *2* (5), a002147.

(7) Godinho, M.; Canejo, J.; Pinto, L.; Borges, J.; Teixeira, P. How to mimic the shapes of plant tendrils on the nano and microscale: spirals and helices of electrospun liquid crystalline cellulose derivatives. *Soft Matter* **2009**, *5* (14), 2772−2776.

(8) Ueshima, R.; Asami, T. Single-gene speciation by left−right reversal. *Nature* **2003**, *425* (6959), 679−679.

(9) Bada, J. L.; Mitchell, E.; Kemper, B. Aspartic acid racemization in narwhal teeth. *Nature* **1983**, *303* (5916), 418−420. Silverman, H.; Dunbar, M. Aggressive tusk use by the narwhal (Monodon monoceros L.). *Nature* **1980**, *284* (5751), 57−58.

(10) Usov, I.; Nyström, G.; Adamcik, J.; Handschin, S.; Schütz, C.; Fall, A.; Bergström, L.; Mezzenga, R. Understanding nanocellulose chirality and structure−properties relationship at the single fibril level. *Nat. commun.* **2015**, *6* (1), 1−11.

(11) Nystrom, G.; Arcari, M.; Adamcik, J.; Usov, I.; Mezzenga, R. Nanocellulose fragmentation mechanisms and inversion of chirality from the single particle to the cholesteric phase. *ACS Nano* **2018**, *12* (6), 5141−5148.

(12) Jin, S.-A.; Facchine, E. G.; Khan, S. A.; Rojas, O. J.; Spontak, R. J. Mesophase characteristics of cellulose nanocrystal films prepared from electrolyte suspensions. *J. Colloid Interface Sci.* **2021**, *599*, 207−218.

(13) Duan, C.; Cheng, Z.; Wang, B.; Zeng, J.; Xu, J.; Li, J.; Gao, W.; Chen, K. Chiral photonic liquid crystal films derived from cellulose nanocrystals. *Small* **2021**, *17* (30), 2007306.

(14) Casado, U.; Mucci, V. L.; Aranguren, M. I. Cellulose nanocrystals suspensions: Liquid crystal anisotropy, rheology and films iridescence. *Carbohydr. Polym.* **2021**, *261*, 117848.

(15) Qing, X.; Liu, Y.; Wei, J.; Zheng, R.; Zhu, C.; Yu, Y. Phototunable Morpho Butterfly Microstructures Modified by Liquid Crystal Polymers. *Adv. Opt. Mater.* **2019**, *7* (3), 1801494.

(16) Goto, H.; Komaba, K.; Kumai, R. Sequential micro-Maltese cross array in the ground beetle Carabus insulicola. *Micron* **2021**, *150*, 103136.

(17) Yoshino, K.; Shimoda, Y.; Kawagishi, Y.; Nakayama, K.; Ozaki, M. Temperature tuning of the stop band in transmission spectra of liquid-crystal infiltrated synthetic opal as tunable photonic crystal. *Appl. Phys. Lett.* **1999**, 75 (7), 932−934.

(18) Prum, R. O.; Torres, R. H. Structural colouration of mammalian skin: convergent evolution of coherently scattering dermal collagen arrays. *J. Exp. Biology* **2004**, 207 (12), 2157−2172.

(19) Chung, K.; Yu, S.; Heo, C.-J.; Shim, J. W.; Yang, S.-M.; Han, M. G.; Lee, H.-S.; Jin, Y.; Lee, S. Y.; Park, N.; Shin, J. H. Flexible, angle-independent, structural color reflectors inspired by Morpho butterfly wings. *Adv. Mater.* **2012**, 24 (18), 2375−2379.

(20) McKenna, D. D.; Scully, E. D.; Pauchet, Y.; Hoover, K.; Kirsch, R.; Geib, S. M.; Mitchell, R. F.; Waterhouse, R. M.; Ahn, S.-J.; Arsala, D.; et al. Genome of the Asian longhorned beetle (Anoplophora glabripennis), a globally significant invasive species, reveals key functional and evolutionary innovations at the beetle−plant interface. *Genome Biol.* **2016**, 17 (1), 1−18.

(21) Mohd-Noor, S.; Jang, H.; Baek, K.; Pei, Y.-R.; Alam, A.-M.; Kim, Y. H.; Kim, I. S.; Choy, J.-H.; Hyun, J. K. Ultrafast humidity-responsive structural colors from disordered nanoporous titania microspheres. *J. Mater. Chem. A* **2019**, 7 (17), 10561−10571. Wilts, B. D.; Mothander, K.; Kelber, A. Humidity-dependent colour change in the green forester moth, Adscita statices, *Biol. Lett.* **2019**, 15 (9), 20190516.

(22) Belmonte, A.; Ussembayev, Y. Y.; Bus, T.; Nys, I.; Neyts, K.; Schenning, A. P. Dual light and temperature responsive micrometer-sized structural color actuators. *Small* **2020**, 16 (1), 1905219.

(23) Qin, M.; Sun, M.; Hua, M.; He, X. Bioinspired structural color sensors based on responsive soft materials. *Curr. Opin. Solid State Mater. Sci.* **2019**, 23 (1), 13−27.

(24) Toriumi, H.; Yahagi, K.; Uematsu, I.; Uematsu, Y. Cholesteric Structure of Lyotropic Poly (I³-benzyl L-glutamate) Liquid Crystals. *Mol. Cryst. Liq. Cryst.* **1983**, 94, 267.

(25) Tang, K.; Green, M. M.; Cheon, K. S.; Selinger, J. V.; Garetz, B. A. Chiral conflict. The effect of temperature on the helical sense of a polymer controlled by the competition between structurally different enantiomers: from dilute solution to the lyotropic liquid crystal state. *J. Am. Chem. Soc.* **2003**, 125 (24), 7313−7323.

(26) Zhang, H.; Bu, X.; Yip, S.; Liang, X.; Ho, J. C. Self-Assembly of Colloidal Particles for Fabrication of Structural Color Materials toward Advanced Intelligent Systems. *Adv. Intell. Syst.* **2020**, 2 (1), 1900085.

(27) Ovsiannikov, D.; Selinski, S.; Lehmann, M.-L.; Blaszkewicz, M.; Moormann, O.; Haenel, M. W.; Hengstler, J. G.; Golka, K. Polymorphic enzymes, urinary bladder cancer risk, and structural change in the local industry. *J.Toxicol. Environ. Health Part A* **2012**, 75 (8–10), 557−565.

(28) Shen, H.; Lin, Q.; Tang, H.; Tian, Y.; Zhang, X. Fabrication of Temperature-and Alcohol-Responsive Photonic Crystal Hydrogel and Its Application for Sustained Drug Release. *Langmuir* **2022**, 38 (12), 3785−3794.

(29) Cathell, M. D.; Schauer, C. L. Structurally colored thin films of Ca2+-cross-linked alginate. *Biomacromolecules* **2007**, 8 (1), 33−41.

(30) Hong, W.; Yuan, Z.; Chen, X. Structural color materials for optical anticounterfeiting. *Small* **2020**, 16 (16), 1907626.

(31) Yablonovitch, E. Liquid versus photonic crystals. *Nature* **1999**, 401 (6753), 539−541.

(32) Cubukcu, E.; Aydin, K.; Ozbay, E.; Foteinopoulou, S.; Soukoulis, C. M. Negative refraction by photonic crystals. *Nature* **2003**, 423 (6940), 604−605. Krauss, T. F. Slow light in photonic crystal waveguides. *J. Phys. D Appl. Phys.* **2007**, 40 (9), 2666.

(33) Jewell, S. A.; Vukusic, P.; Roberts, N. Circularly polarized colour reflection from helicoidal structures in the beetle Plusiotis boucardi. *New J. Phys.* **2007**, 9 (4), 99.

(34) Kose, O.; Tran, A.; Lewis, L.; Hamad, W. Y.; MacLachlan, M. J. Unwinding a spiral of cellulose nanocrystals for stimuli-responsive stretchable optics. *Nat. Commun.* **2019**, 10 (1), 1−7.

(35) Onsager, L. The effects of shape on the interaction of colloidal particles. *Ann. N.Y. Acad. Sci.* **1949**, 51 (4), 627−659.

(36) Duggal, R.; Pasquali, M. Dynamics of individual single-walled carbon nanotubes in water by real-time visualization. *Phys. rev. lett.* **2006**, 96 (24), 246104.

(37) Fakhri, N.; Tsyboulski, D. A.; Cognet, L.; Weisman, R. B.; Pasquali, M. Diameter-dependent bending dynamics of single-walled carbon nanotubes in liquids. *Proc. Natl. Acad. Sci. U. S. A.* **2009**, 106 (34), 14219−14223.

(38) Morse, D. C. Tube diameter in tightly entangled solutions of semiflexible polymers. *Phys. Rev. E* **2001**, 63 (3), 031502.

(39) Doi, M.; Edwards, S. F.; Edwards, S. F. *The theory of polymer dynamics*; Oxford University Press, 1988.

(40) Hough, L.; Islam, M.; Janmey, P.; Yodh, A. Viscoelasticity of single wall carbon nanotube suspensions. *Phys. rev. lett.* **2004**, 93 (16), 168102.

(41) Fraden, S.; Hurd, A.; Meyer, R.; Cahoon, M.; Caspar, D. Magnetic-field-induced alignment and instabilities in ordered colloids of tobacco mosaic virus. *Le. J. Phys. Colloq.* **1985**, 46 (C3), C3−85−C83−113.

(42) Kang, K.; Dhont, J. Glass transition in suspensions of charged rods: structural arrest and texture dynamics. *Phys. rev. lett.* **2013**, 110 (1), 015901. Kang, K.; Dhont, J. K. Electric-field induced transitions in suspensions of charged colloidal rods. *Soft Matter* **2010**, 6 (2), 273−286.

(43) Missana, T.; Adell, A. On the applicability of DLVO theory to the prediction of clay colloids stability. *J. Colloid Interface Sci.* **2000**, 230 (1), 150−156.

(44) Singh, A.; Ness, C.; Seto, R.; de Pablo, J. J.; Jaeger, H. M. Shear thickening and jamming of dense suspensions: the "roll" of friction. *Phys. rev. lett.* **2020**, 124 (24), 248005.

(45) Stradner, A.; Sedgwick, H.; Cardinaux, F.; Poon, W. C.; Egelhaaf, S. U.; Schurtenberger, P. Equilibrium cluster formation in concentrated protein solutions and colloids. *Nature* **2004**, 432 (7016), 492−495.

(46) Pham, K. N.; Puertas, A. M.; Bergenholtz, J.; Egelhaaf, S. U.; Moussaïd, A.; Pusey, P. N.; Schofield, A. B.; Cates, M. E.; Fuchs, M.; Poon, W. C. Multiple glassy states in a simple model system. *Science* **2002**, 296 (5565), 104−106.

(47) Abbasi Moud, A. Gel development using cellulose nanocrystals. *PhD (Thesis)*; University of Calgary, 2020. Moud, A. A.; Arjmand, M.; Liu, J.; Yang, Y.; Sanati-Nezhad, A.; Hejazi, S. H. Cellulose nanocrystal structure in the presence of salts. *Cellulose* **2019**, 26 (18), 9387−9401. Moud, A. A.; Arjmand, M.; Yan, N.; Nezhad, A. S.; Hejazi, S. H. Colloidal behavior of cellulose nanocrystals in presence of sodium chloride. *ChemistrySelect* **2018**, 3 (17), 4969−4978.

(48) Santos, A.; Lopez de Haro, M.; Fiumara, G.; Saija, F. The effective colloid interaction in the Asakura−Oosawa model. Assessment of non-pairwise terms from the virial expansion. *J. Chem. Phys.* **2015**, 142 (22), 224903.

(49) Asakura, S.; Oosawa, F. Interaction between particles suspended in solutions of macromolecules. *J. Polym. Sci.* **1958**, 33 (126), 183−192.

(50) Bai, L.; Huan, S.; Xiang, W.; Rojas, O. J. Pickering emulsions by combining cellulose nanofibrils and nanocrystals: Phase behavior and depletion stabilization. *Green Chem.* **2018**, 20 (7), 1571−1582.

(51) Sun, X.; Danumah, C.; Liu, Y.; Boluk, Y. Flocculation of bacteria by depletion interactions due to rod-shaped cellulose nanocrystals. *Chem. eng. j.* **2012**, 198, 476−481. Sun, X.; Shao, Y.; Boluk, Y.; Liu, Y. The impact of cellulose nanocrystals on the aggregation and initial adhesion to a solid surface of Escherichia coli K12: Role of solution chemistry. *Colloids Surf., B* **2015**, 136, 570−576.

(52) Lekkerkerker, H. N.; Tuinier, R. Depletion interaction. In *Colloids and the depletion interaction*; Springer, 2011; pp 57−108.

(53) Oster, G. Two-phase formation in solutions of tobacco mosaic virus and the problem of long-range forces. *J. gen. physiol.* **1950**, 33 (5), 445−473.

(54) Dogic, Z.; Fraden, S. Cholesteric phase in virus suspensions. *Langmuir* **2000**, 16 (20), 7820−7824.

(55) Leforestier, A.; Bertin, A.; Dubochet, J.; Richter, K.; Blanc, N. S.; Livolant, F. Expression of chirality in columnar hexagonal phases or DNA and nucleosomes. *C. R. Chim.* **2008**, 11 (3), 229−244.

(56) Folda, T.; Hoffmann, H.; Chanzy, H.; Smith, P. *Nature* **1988**, 333, 55.

(57) Barry, E.; Hensel, Z.; Dogic, Z.; Shribak, M.; Oldenbourg, R. Entropy-driven formation of a chiral liquid-crystalline phase of helical filaments. *Phys. rev. lett.* **2006**, *96* (1), 018305.

(58) Giraud-Guille, M.-M. Twisted plywood architecture of collagen fibrils in human compact bone osteons. *Calcif. Tissue Int.* **1988**, *42* (3), 167−180.

(59) Buining, P.; Lekkerkerker, H. Isotropic-nematic phase separation of a dispersion of organophilic boehmite rods. *J. Phys. Chem.* **1993**, *97* (44), 11510−11516.

(60) Chan, C. L. C.; Bay, M. M.; Jacucci, G.; Vadrucci, R.; Williams, C. A.; van de Kerkhof, G. T.; Parker, R. M.; Vynck, K.; Frka-Petesic, B.; Vignolini, S. Visual Appearance of Chiral Nematic Cellulose-Based Photonic Films: Angular and Polarization Independent Color Response with a Twist. *Adv. Mater.* **2019**, *31* (52), 1905151.

(61) Revol, J.-F.; Marchessault, R. In vitro chiral nematic ordering of chitin crystallites. *Int. J. Biol. Macromol.* **1993**, *15* (6), 329−335.

(62) Borgström, J.; Quist, P.; Piculell, L. *Macromolecules* **1996**, *29*, 5926−5933.

(63) DuPré, D. B.; Duke, R. W. Temperature, concentration, and molecular weight dependence of the twist elastic constant of cholesteric poly-γ-benzyl-L-glutamate. *J. chem. phys.* **1975**, *63* (1), 143−148.

(64) Livolant, F.; Bouligand, Y. Liquid crystalline phases given by helical biological polymers (DNA, PBLG and xanthan). Columnar textures. *J. phys.* **1986**, *47* (10), 1813−1827.

(65) Grelet, E.; Fraden, S. What is the origin of chirality in the cholesteric phase of virus suspensions? *Phys. rev. lett.* **2003**, *90* (19), 198302.

(66) Marchessault, R.; Morehead, F.; Koch, M. J. Some hydrodynamic properties of neutral suspensions of cellulose crystallites as related to size and shape. *J. Colloid Sci.* **1961**, *16* (4), 327−344. Marchessault, R.; Morehead, F.; Walter, N. Liquid crystal systems from fibrillar polysaccharides. *Nature* **1959**, *184* (4686), 632−633.

(67) Werbowyj, R. S.; Gray, D. G. Liquid crystalline state of concentrated solution cyanoethyl derivatives. *Mol. Cryst. Liq. Crys. Lett.* **1976**, *34*, 97.

(68) Revol, J.-F.; Bradford, H.; Giasson, J.; Marchessault, R.; Gray, D. Helicoidal self-ordering of cellulose microfibrils in aqueous suspension. *Int. J. Biol. Macromol.* **1992**, *14* (3), 170−172.

(69) Revol, J.-F.; Godbout, L.; Dong, X.-M.; Gray, D. G.; Chanzy, H.; Maret, G. Chiral nematic suspensions of cellulose crystallites; phase separation and magnetic field orientation. *Liq. Cryst.* **1994**, *16* (1), 127−134.

(70) Kopp, V.; Fan, B.; Vithana, H.; Genack, A. Low-threshold lasing at the edge of a photonic stop band in cholesteric liquid crystals. *Optics lett.* **1998**, *23* (21), 1707−1709.

(71) Palffy-Muhoray, P.; Cao, W.; Moreira, M.; Taheri, B.; Munoz, A. Photonics and lasing in liquid crystal materials. *Philos. Trans. R. Soc. Math. Phys. Eng. Sci.* **2006**, *364* (1847), 2747−2761.

(72) Wilts, B.; Dumanli, A. G.; Middleton, R.; Vukusic, P.; Vignolini, S. Invited Article: Chiral optics of helicoidal cellulose nanocrystal films. *APL Photonics* **2017**, *2* (4), 040801.

(73) Wang, P.-X.; Hamad, W. Y.; MacLachlan, M. J. Structure and transformation of tactoids in cellulose nanocrystal suspensions. *Nat. Commun.* **2016**, *7* (1), 1−8.

(74) Schutz, C.; Agthe, M.; Fall, A. B.; Gordeyeva, K.; Guccini, V.; Salajková, M.; Plivelic, T. S.; Lagerwall, J. P.; Salazar-Alvarez, G.; Bergstrom, L. Rod packing in chiral nematic cellulose nanocrystal dispersions studied by small-angle X-ray scattering and laser diffraction. *Langmuir* **2015**, *31* (23), 6507−6513.

(75) Dong, X. M.; Kimura, T.; Revol, J.-F.; Gray, D. G. Effects of ionic strength on the isotropic− chiral nematic phase transition of suspensions of cellulose crystallites. *Langmuir* **1996**, *12* (8), 2076−2082.

(76) Hirai, A.; Inui, O.; Horii, F.; Tsuji, M. Phase separation behavior in aqueous suspensions of bacterial cellulose nanocrystals prepared by sulfuric acid treatment. *Langmuir* **2009**, *25* (1), 497−502.

(77) Gray, D. Chiral nematic ordering of polysaccharides. *Carbohydr. Polym.* **1994**, *25* (4), 277−284.

(78) Orts, W.; Revol, J.-F.; Godbout, L.; Marchessault, R. SANS study of chirality and order in liquid crystalline cellulose suspensions. *MRS Online Proc. Libr. (OPL)* **1994**, *376*, 317.

(79) Orts, W. J.; Godbout, L.; Marchessault, R. H.; Revol, J.-F. Enhanced ordering of liquid crystalline suspensions of cellulose microfibrils: a small angle neutron scattering study. *Macromolecules* **1998**, *31* (17), 5717−5725.

(80) Araki, J.; Kuga, S. Effect of trace electrolyte on liquid crystal type of cellulose microcrystals. *Langmuir* **2001**, *17* (15), 4493−4496.

(81) Araki, J.; Wada, M.; Kuga, S.; Okano, T. Flow properties of microcrystalline cellulose suspension prepared by acid treatment of native cellulose. *Colloids Surf., A* **1998**, *142* (1), 75−82.

(82) Lenfant, G.; Heuzey, M.-C.; van de Ven, T. G. M.; Carreau, P. J. A comparative study of ECNC and CNC suspensions: effect of salt on rheological properties. *Rheol. Acta* **2017**, *56* (1), 51−62. Cherhal, F.; Cousin, F.; Capron, I. Influence of charge density and ionic strength on the aggregation process of cellulose nanocrystals in aqueous suspension, as revealed by small-angle neutron scattering. *Langmuir* **2015**, *31* (20), 5596−5602.

(83) Edwards, S.; Evans, K. Dynamics of highly entangled rod-like molecules. *J. Chem. Soc. Faraday Trans. 2* **1982**, *78* (1), 113−121.

(84) Krall, A.; Weitz, D. Internal dynamics and elasticity of fractal colloidal gels. *Phys. rev. lett.* **1998**, *80* (4), 778.

(85) Conley, K.; Whitehead, M.; van de Ven, T. G. Probing the structural chirality of crystalline cellulose with induced circular dichroism. *Cellulose* **2017**, *24* (2), 479−486.

(86) Hanley, S. J.; Revol, J.-F.; Godbout, L.; Gray, D. G. Atomic force microscopy and transmission electron microscopy of cellulose from Micrasterias denticulata; evidence for a chiral helical microfibril twist. *Cellulose* **1997**, *4* (3), 209−220.

(87) Elazzouzi-Hafraoui, S.; Nishiyama, Y.; Putaux, J.-L.; Heux, L.; Dubreuil, F.; Rochas, C. The shape and size distribution of crystalline nanoparticles prepared by acid hydrolysis of native cellulose. *Biomacromolecules* **2008**, *9* (1), 57−65.

(88) Matthews, J. F.; Skopec, C. E.; Mason, P. E.; Zuccato, P.; Torget, R. W.; Sugiyama, J.; Himmel, M. E.; Brady, J. W. Computer simulation studies of microcrystalline cellulose Iβ. *Carbohydr. Res.* **2006**, *341* (1), 138−152.

(89) Werbowyj, R. S.; Gray, D. G. Optical properties of hydroxypropyl cellulose liquid crystals. I. Cholesteric pitch and polymer concentration. *Macromolecules* **1984**, *17* (8), 1512−1520.

(90) Dumanli, A. G.; Kamita, G.; Landman, J.; van der Kooij, H.; Glover, B. J.; Baumberg, J. J.; Steiner, U.; Vignolini, S. Controlled, bio-inspired self-assembly of cellulose-based chiral reflectors. *Adv. Opt. Mater.* **2014**, *2* (7), 646−650.

(91) Dumanli, A. G. m.; Van Der Kooij, H. M.; Kamita, G.; Reisner, E.; Baumberg, J. J.; Steiner, U.; Vignolini, S. Digital color in cellulose nanocrystal films. *ACS appl. mater. interface* **2014**, *6* (15), 12302−12306.

(92) De Vries, H. Rotatory power and other optical properties of certain liquid crystals. *Acta Crystallogr.* **1951**, *4* (3), 219−226. Nguyen, T.-D.; Sierra, E.; Eguiraun, H.; Lizundia, E. Iridescent cellulose nanocrystal films: the link between structural colour and Bragg's law. *Eur. J. Phys.* **2018**, *39* (4), 045803.

(93) Lagerwall, S. T. On some important chapters in the history of liquid crystals. *Liq. Cryst.* **2013**, *40* (12), 1698−1729.

(94) Tran, A.; Boott, C. E.; MacLachlan, M. J. Understanding the Self-Assembly of Cellulose Nanocrystals—Toward Chiral Photonic Materials. *Adv. Mater.* **2020**, *32* (41), 1905876.

(95) Honorato-Rios, C.; Kuhnhold, A.; Bruckner, J. R.; Dannert, R.; Schilling, T.; Lagerwall, J. P. Equilibrium liquid crystal phase diagrams and detection of kinetic arrest in cellulose nanocrystal suspensions. *Front. Mater.* **2016**, 21.

(96) Shafiei-Sabet, S.; Hamad, W.; Hatzikiriakos, S. Ionic strength effects on the microstructure and shear rheology of cellulose nanocrystal suspensions. *Cellulose* **2014**, *21* (5), 3347−3359.

(97) Parker, R. M.; Frka-Petesic, B.; Guidetti, G.; Kamita, G.; Consani, G.; Abell, C.; Vignolini, S. Hierarchical self-assembly of cellulose

nanocrystals in a confined geometry. *ACS Nano* **2016**, *10* (9), 8443−8449.

(98) Guidetti, G.; Atifi, S.; Vignolini, S.; Hamad, W. Y. Flexible photonic cellulose nanocrystal films. *Adv. Mater.* **2016**, *28* (45), 10042−10047.

(99) Solomon, M. J.; Spicer, P. T. Microstructural regimes of colloidal rod suspensions, gels, and glasses. *Soft Matter* **2010**, *6* (7), 1391−1400.

(100) Schütz, C.; Bruckner, J. R.; Honorato-Rios, C.; Tosheva, Z.; Anyfantakis, M.; Lagerwall, J. P. From equilibrium liquid crystal formation and kinetic arrest to photonic bandgap films using suspensions of cellulose nanocrystals. *Crystals* **2020**, *10* (3), 199.

(101) Hartmann, R.; Kinnunen, P.; Illikainen, M. Cellulose-mineral interactions based on the DLVO theory and their correlation with flotability. *Miner. Eng.* **2018**, *122*, 44−52.

(102) Oguzlu, H.; Danumah, C.; Boluk, Y. Colloidal behavior of aqueous cellulose nanocrystal suspensions. *Curr. Opin. Colloid Interface Sci.* **2017**, *29*, 46−56.

(103) Lin, M.; Raghuwanshi, V. S.; Browne, C.; Simon, G. P.; Garnier, G. Modulating transparency and colour of cellulose nanocrystal composite films by varying polymer molecular weight. *J. Colloid Interface Sci.* **2021**, *584*, 216−224.

(104) Jia, W.; Liu, Y. Two characteristic cellulose nanocrystals (CNCs) obtained from oxalic acid and sulfuric acid processing. *Cellulose* **2019**, *26* (15), 8351−8365.

(105) Zheng, H.; Li, W.; Li, W.; Wang, X.; Tang, Z.; Zhang, S. X. A.; Xu, Y. Uncovering the circular polarization potential of chiral photonic cellulose films for photonic applications. *Adv. Mater.* **2018**, *30* (13), 1705948.

(106) Li, C.; Evans, J.; Wang, N.; Guo, T.; He, S. pH dependence of the chirality of nematic cellulose nanocrystals. *Sci. Rep.* **2019**, *9* (1), 1−7.

(107) Cheng, Z.; Ma, Y.; Yang, L.; Cheng, F.; Huang, Z.; Natan, A.; Li, H.; Chen, Y.; Cao, D.; Huang, Z.; et al. Plasmonic-Enhanced Cholesteric Films: Coassembling Anisotropic Gold Nanorods with Cellulose Nanocrystals. *Adv. Opt. Mater.* **2019**, *7* (9), 1801816.

(108) Xu, Y.-T.; Li, J.; MacLachlan, M. J. Stable graphene oxide hydrophobic photonic liquids. *Nanoscale Horiz.* **2022**, DOI: 10.1039/D1NH00523E.

(109) Oguzlu, H.; Danumah, C.; Boluk, Y. The role of dilute and semi-dilute cellulose nanocrystal (CNC) suspensions on the rheology of carboxymethyl cellulose (CMC) solutions. *Can. J. Chem. Eng.* **2016**, *94* (10), 1841−1847.

(110) Edgar, C. D.; Gray, D. G. Influence of dextran on the phase behavior of suspensions of cellulose nanocrystals. *Macromolecules* **2002**, *35* (19), 7400−7406.

(111) Shim, Y. H.; Lee, K. E.; Shin, T. J.; Kim, S. O.; Kim, S. Y. Tailored colloidal stability and rheological properties of graphene oxide liquid crystals with polymer-induced depletion attractions. *ACS Nano* **2018**, *12* (11), 11399−11406.

(112) Sung, B.; Wensink, H. H.; Grelet, E. Depletion-driven morphological transitions in hexagonal crystallites of virus rods. *Soft Matter* **2019**, *15* (46), 9520−9527.

(113) Parker, R. M.; Guidetti, G.; Williams, C. A.; Zhao, T.; Narkevicius, A.; Vignolini, S.; Frka-Petesic, B. The self-assembly of cellulose nanocrystals: Hierarchical design of visual appearance. *Adv. Mater.* **2018**, *30* (19), 1704477.

(114) Müller, D.; Kampmann, T. A.; Kierfeld, J. Chaining of hard disks in nematic needles: particle-based simulation of colloidal interactions in liquid crystals. *Sci. Rep.* **2020**, *10* (1), 1−12.

(115) Petukhov, A. V.; Tuinier, R.; Vroege, G. J. Entropic patchiness: Effects of colloid shape and depletion. *Curr. Opin. Colloid Interface Sci.* **2017**, *30*, 54−61.

(116) Yamaguchi, N.; Anraku, S.; Paineau, E.; Safinya, C. R.; Davidson, P.; Michot, L. J.; Miyamoto, N. Swelling inhibition of liquid crystalline colloidal montmorillonite and beidellite clays by DNA. *Sci. Rep.* **2018**, *8* (1), 1−13.

(117) Wang, Y.; Chen, Z.; Tang, J.; Lin, N. Tunable Optical Materials Based on Self-assembly of Polysaccharide Nanocrystals. In *Advanced Functional Materials from Nanopolysaccharides*; Springer, 2019; pp 87−

136. Zhang, Y.; Tian, Z.; Fu, Y.; Wang, Z.; Qin, M.; Yuan, Z. Responsive and patterned cellulose nanocrystal films modified by N-methylmorpholine-N-oxide. *Carbohydr. Polym.* **2020**, *228*, 115387.

(118) Bardet, R.; Belgacem, N.; Bras, J. Flexibility and color monitoring of cellulose nanocrystal iridescent solid films using anionic or neutral polymers. *ACS appl. mater. interface* **2015**, *7* (7), 4010−4018. Reid, M. S.; Villalobos, M.; Cranston, E. D. The role of hydrogen bonding in non-ionic polymer adsorption to cellulose nanocrystals and silica colloids. *Curr. Opin. Colloid Interface Sci.* **2017**, *29*, 76−82.

(119) Cao, Y.; Hamad, W. Y.; MacLachlan, M. J. Broadband circular polarizing film based on chiral nematic liquid crystals. *Adv. Opt. Mater.* **2018**, *6* (17), 1800412.

(120) Rogowski, R. The kinetics of nucleation in inhomogeneous media based on the classical Avrami model. *Mater. Sci.* **2005**, *23* (4).

(121) Thérien-Aubin, H.; Lukach, A.; Pitch, N.; Kumacheva, E. Coassembly of nanorods and nanospheres in suspensions and in stratified films. *Angew. Chem.* **2015**, *127* (19), 5710−5714. Thérien-Aubin, H.; Lukach, A.; Pitch, N.; Kumacheva, E. Structure and properties of composite films formed by cellulose nanocrystals and charged latex nanoparticles. *Nanoscale* **2015**, *7* (15), 6612−6618.

(122) Sadati, M.; Apik, A. I.; Armas-Perez, J. C.; Martinez-Gonzalez, J.; Hernandez-Ortiz, J. P.; Abbott, N. L.; de Pablo, J. J. Liquid crystal enabled early stage detection of beta amyloid formation on lipid monolayers. *Adv. Funct. Mater.* **2015**, *25* (38), 6050−6060. Lowe, A. M.; Abbott, N. L. Liquid crystalline materials for biological applications. *Chem. Mater.* **2012**, *24* (5), 746−758.

(123) Yao, K.; Meng, Q.; Bulone, V.; Zhou, Q. Flexible and responsive chiral nematic cellulose nanocrystal/poly (ethylene glycol) composite films with uniform and tunable structural color. *Adv. Mater.* **2017**, *29* (28), 1701323.

(124) Honorato-Rios, C.; Lehr, C.; Schütz, C.; Sanctuary, R.; Osipov, M. A.; Baller, J.; Lagerwall, J. P. Fractionation of cellulose nanocrystals: enhancing liquid crystal ordering without promoting gelation. *NPG Asia Mater.* **2018**, *10* (5), 455−465.

(125) Timbrell, V. Alignment of carbon and other man-made fibers by magnetic fields. *J. Appl. Phys.* **1972**, *43* (11), 4839−4840. Schmitt, Y.; Paulick, C.; Royer, F.; Gasser, J. Magnetic field induced orientational order of conductive fibers in non-conductive liquids. *J. non-crystalline solid* **1996**, *205*, 135−138.

(126) Fujiwara, M.; Oki, E.; Hamada, M.; Tanimoto, Y.; Mukouda, I.; Shimomura, Y. Magnetic orientation and magnetic properties of a single carbon nanotube. *J. phys. chem. A* **2001**, *105* (18), 4383−4386.

(127) Kimura, T.; Yamato, M.; Koshimizu, W.; Koike, M.; Kawai, T. Magnetic orientation of polymer fibers in suspension. *Langmuir* **2000**, *16* (2), 858−861.

(128) Dong, X.; Kimura, T.; Revol, J.; Gray, D. *Langmuir* **1996**, *12*, 2076−2082. Araki, J.; Wada, M.; Kuga, S.; Okano, T. *Langmuir* **2000**, *16*, 2413−2415.

(129) Vignolini, S. Cellulose nanocrystal holograms. *APS March Meeting Abstracts* **2021**, *2021*, B09.

(130) Kimura, F.; Kimura, T.; Tamura, M.; Hirai, A.; Ikuno, M.; Horii, F. Magnetic alignment of the chiral nematic phase of a cellulose microfibril suspension. *Langmuir* **2005**, *21* (5), 2034−2037.

(131) Sharif, F.; Arjmand, M.; Moud, A. A.; Sundararaj, U.; Roberts, E. P. Segregated hybrid poly (methyl methacrylate)/graphene/magnetite nanocomposites for electromagnetic interference shielding. *ACS appl. mater. interface* **2017**, *9* (16), 14171−14179.

(132) Barhoumi Meddeb, A.; Chae, I.; Han, A.; Kim, S. H.; Ounaies, Z. Magnetic field effects on cellulose nanocrystal ordering in a non-aqueous solvent. *Cellulose* **2020**, *27* (14), 7901−7910.

(133) Moud, A. A. Fluorescence Recovery after Photobleaching in Colloidal Science: Introduction and Application. *ACS Biomater. Sci. Eng.* **2022**, *8* (3), 1028−1048.

(134) Habibi, Y.; Heim, T.; Douillard, R. AC electric field-assisted assembly and alignment of cellulose nanocrystals. *J. Polym. Sci., Part B: Polym. Phys.* **2008**, *46* (14), 1430−1436.

(135) Mun, S. J.; Shim, Y. H.; Kim, G. W.; Koo, S. H.; Ahn, H.; Shin, T. J.; Kim, S. O.; Kim, S. Y. Tailored growth of graphene oxide liquid

crystals with controlled polymer crystallization in GO-polymer composites. *Nanoscale* **2021**, *13* (4), 2720−2727.

(136) Dozov, I.; Paineau, E.; Davidson, P.; Antonova, K.; Baravian, C.; Bihannic, I.; Michot, L. Electric-field-induced perfect anti-nematic order in isotropic aqueous suspensions of a natural beidellite clay. *J. Phys. Chem. B* **2011**, *115* (24), 7751−7765.

(137) Inadomi, T.; Ikeda, S.; Okumura, Y.; Kikuchi, H.; Miyamoto, N. Photo-Induced Anomalous Deformation of Poly (N-Isopropylacrylamide) Gel Hybridized with an Inorganic Nanosheet Liquid Crystal Aligned by Electric Field. *Macromol. Rapid Commun.* **2014**, *35* (20), 1741−1746.

(138) De France, K. J.; Yager, K. G.; Hoare, T.; Cranston, E. D. Cooperative ordering and kinetics of cellulose nanocrystal alignment in a magnetic field. *Langmuir* **2016**, *32* (30), 7564−7571.

(139) Frka-Petesic, B.; Sugiyama, J.; Kimura, S.; Chanzy, H.; Maret, G. Negative diamagnetic anisotropy and birefringence of cellulose nanocrystals. *Macromolecules* **2015**, *48* (24), 8844−8857.

(140) Kim, J. E.; Han, T. H.; Lee, S. H.; Kim, J. Y.; Ahn, C. W.; Yun, J. M.; Kim, S. O. Graphene oxide liquid crystals. *Angew. Chem.* **2011**, *123* (13), 3099−3103.

(141) Hull, R.; Hills, G.; Markham, R. Studies on Alfalfa mosaic virus: II. The structure of the virus components. *Virology* **1969**, *37* (3), 416−428. He, Q.-Q.; Lan, Y.; Quan, Y.-Y.; Li, C.-Y.; Liu, Y.-P.; Wang, X.-J.; Jia, Y.-G.; Tian, M.; Yao, D.-S. The influence of the structure of terminal groups and cores on the properties of schiff base star-shaped liquid crystals. *Liq. Cryst.* **2021**, *48* (9), 1309−1320.

(142) Li, P.; Wong, M.; Zhang, X.; Yao, H.; Ishige, R.; Takahara, A.; Miyamoto, M.; Nishimura, R.; Sue, H.-J. Tunable lyotropic photonic liquid crystal based on graphene oxide. *ACS photonics* **2014**, *1* (1), 79−86.

(143) Hong, S.-H.; Shen, T.-Z.; Song, J.-K. Manipulation of structural color reflection in graphene oxide dispersions using electric fields. *Opt. Express* **2015**, *23* (15), 18969−18974.

(144) Kvien, I.; Oksman, K. Orientation of cellulose nanowhiskers in polyvinyl alcohol. *Appl. Phys. A: Mater. Sci. Process.* **2007**, *87* (4), 641−643.

(145) Ebeling, T.; Paillet, M.; Borsali, R.; Diat, O.; Dufresne, A.; Cavaille, J.; Chanzy, H. Shear-induced orientation phenomena in suspensions of cellulose microcrystals, revealed by small angle X-ray scattering. *Langmuir* **1999**, *15* (19), 6123−6126. Hoeger, I.; Rojas, O. J.; Efimenko, K.; Velev, O. D.; Kelley, S. S. Ultrathin film coatings of aligned cellulose nanocrystals from a convective-shear assembly system and their surface mechanical properties. *Soft Matter* **2011**, *7* (5), 1957−1967.

(146) Abbasi Moud, A. Cellulose through the lens of microfluidics: a review. *Appl. Biosci.* **2022**, *1* (1), 1−37.

(147) Repula, A.; Oshima Menegon, M.; Wu, C.; van der Schoot, P.; Grelet, E. Directing liquid crystalline self-organization of rodlike particles through tunable attractive single tips. *Phys. Rev. Lett.* **2019**, *122* (12), 128008.

(148) Edgar, C. D.; Gray, D. G. Induced circular dichroism of chiral nematic cellulose films. *Cellulose* **2001**, *8* (1), 5−12.

(149) Giese, M. Imprinting of photonic patterns with thermosetting amino-formaldehyde-cellulose composites. *ACS Macro Lett.* **2013**, *52*, 8921.

(150) Vollick, B.; Kuo, P.-Y.; Therien-Aubin, H.; Yan, N.; Kumacheva, E. Composite cholesteric nanocellulose films with enhanced mechanical properties. *Chem. Mater.* **2017**, *29* (2), 789−795.

(151) Querejeta-Fernández, A.; Chauve, G. g.; Methot, M.; Bouchard, J.; Kumacheva, E. Chiral plasmonic films formed by gold nanorods and cellulose nanocrystals. *J. Am. Chem. Soc.* **2014**, *136* (12), 4788−4793.

(152) Schlesinger, M.; Giese, M.; Blusch, L. K.; Hamad, W. Y.; MacLachlan, M. J. Chiral nematic cellulose−gold nanoparticle composites from mesoporous photonic cellulose. *Chem. Commun.* **2015**, *51* (3), 530−533.

(153) Weaver, J. C.; Milliron, G. W.; Miserez, A.; Evans-Lutterodt, K.; Herrera, S.; Gallana, I.; Mershon, W. J.; Swanson, B.; Zavattieri, P.; DiMasi, E.; et al. The stomatopod dactyl club: a formidable damage-tolerant biological hammer. *Science* **2012**, *336* (6086), 1275−1280.

(154) Bouligand, Y. Liquid crystals and biological morphogenesis: Ancient and new questions. *C. R. Chim.* **2008**, *11* (3), 281−296.

(155) Behera, R. P.; Le Ferrand, H. Impact-resistant materials inspired by the mantis shrimp's dactyl club. *Matter* **2021**, *4* (9), 2831−2849.

(156) Nikolov, S.; Petrov, M.; Lymperakis, L.; Friák, M.; Sachs, C.; Fabritius, H. O.; Raabe, D.; Neugebauer, J. Revealing the design principles of high-performance biological composites using ab initio and multiscale simulations: the example of lobster cuticle. *Adv. Mater.* **2010**, *22* (4), 519−526.

(157) Tripathi, A.; Tardy, B. L.; Khan, S. A.; Liebner, F.; Rojas, O. J. Expanding the upper limits of robustness of cellulose nanocrystal aerogels: outstanding mechanical performance and associated pore compression response of chiral-nematic architectures. *J. Mater. Chem. A* **2019**, *7* (25), 15309−15319.

(158) Wu, T.; Li, J.; Li, J.; Ye, S.; Wei, J.; Guo, J. A bio-inspired cellulose nanocrystal-based nanocomposite photonic film with hyper-reflection and humidity-responsive actuator properties. *J. Mater. Chem. C* **2016**, *4* (41), 9687−9696.

(159) Fernandes, S. N.; Almeida, P. L.; Monge, N.; Aguirre, L. E.; Reis, D.; de Oliveira, C. L.; Neto, A. M.; Pieranski, P.; Godinho, M. H. Mind the microgap in iridescent cellulose nanocrystal films. *Adv. Mater.* **2017**, *29* (2), 1603560.

(160) Liu, D.; Li, J.; Sun, F.; Xiao, R.; Guo, Y.; Song, J. Liquid crystal microphase separation of cellulose nanocrystals in wet-spun PVA composite fibers. *Rsc Adv.* **2014**, *4* (58), 30784−30789.

(161) Mu, X.; Gray, D. G. Droplets of cellulose nanocrystal suspensions on drying give iridescent 3-D "coffee-stain" rings. *Cellulose* **2015**, *22* (2), 1103−1107.

(162) Bardet, R.; Roussel, F.; Coindeau, S.; Belgacem, N.; Bras, J. Engineered pigments based on iridescent cellulose nanocrystal films. *Carbohydr. Polym.* **2015**, *122*, 367−375.

(163) Beck, S.; Bouchard, J. Auto-catalyzed acidic desulfation of cellulose nanocrystals. *Mordic Pulp Pap. Res. J.* **2014**, *29* (1), 6−14.

(164) Nan, F.; Nagarajan, S.; Chen, Y.; Liu, P.; Duan, Y.; Men, Y.; Zhang, J. Enhanced toughness and thermal stability of cellulose nanocrystal iridescent films by alkali treatment. *ACS Sustain. Chem. Eng.* **2017**, *5* (10), 8951−8958.

(165) Park, J. H.; Noh, J.; Schütz, C.; Salazar-Alvarez, G.; Scalia, G.; Bergström, L.; Lagerwall, J. P. Macroscopic control of helix orientation in films dried from cholesteric liquid-crystalline cellulose nanocrystal suspensions. *ChemPhysChem* **2014**, *15* (7), 1477−1484.

(166) de Heer, W. A.; Bacsa, W.; Chatelain, A.; Gerfin, T.; Humphrey-Baker, R.; Forro, L.; Ugarte, D. Aligned carbon nanotube films: production and optical and electronic properties. *Science* **1995**, *268* (5212), 845−847.

(167) Chen, Q.; Liu, P.; Nan, F.; Zhou, L.; Zhang, J. Tuning the iridescence of chiral nematic cellulose nanocrystal films with a vacuum-assisted self-assembly technique. *Biomacromolecules* **2014**, *15* (11), 4343−4350.

(168) Wang, Z.; Li, N.; Zong, L.; Zhang, J. Recent advances in vacuum assisted self-assembly of cellulose nanocrystals. *Curr. Opin. Solid State Mater. Sci.* **2019**, *23* (3), 142−148.

(169) Bercea, M.; Navard, P. Shear dynamics of aqueous suspensions of cellulose whiskers. *Macromolecules* **2000**, *33* (16), 6011−6016.

(170) Ureña-Benavides, E. E.; Ao, G.; Davis, V. A.; Kitchens, C. L. Rheology and phase behavior of lyotropic cellulose nanocrystal suspensions. *Macromolecules* **2011**, *44* (22), 8990−8998.

(171) Shafiei-Sabet, S.; Hamad, W. Y.; Hatzikiriakos, S. G. Rheology of nanocrystalline cellulose aqueous suspensions. *Langmuir* **2012**, *28* (49), 17124−17133.

(172) González-Labrada, E.; Gray, D. G. Viscosity measurements of dilute aqueous suspensions of cellulose nanocrystals using a rolling ball viscometer. *Cellulose* **2012**, *19* (5), 1557−1565.

(173) Boluk, Y.; Lahiji, R.; Zhao, L.; McDermott, M. T. Suspension viscosities and shape parameter of cellulose nanocrystals (CNC). *Colloids Surf., A* **2011**, *377* (1−3), 297−303.

(174) Kundu, S.; Ogale, A. A. Microstructural effects on the dynamic rheology of a discotic mesophase pitch. *Rheol. Acta* **2007**, *46* (9), 1211−1222.

(175) Xu, Z.; Gao, C. Aqueous liquid crystals of graphene oxide. *ACS Nano* **2011**, 5 (4), 2908–2915.

(176) Yang, X.; Guo, C.; Ji, L.; Li, Y.; Tu, Y. Liquid crystalline and shear-induced properties of an aqueous solution of graphene oxide sheets. *Langmuir* **2013**, 29 (25), 8103–8107.

(177) Hong, S.-H.; Shen, T.-Z.; Song, J.-K. Flow-induced ordering of particles and flow velocity profile transition in a tube flow of graphene oxide dispersions. *Liq. Cryst.* **2015**, 42 (2), 261–269.

(178) Naficy, S.; Jalili, R.; Aboutalebi, S. H.; Gorkin, R. A., III; Konstantinov, K.; Innis, P. C.; Spinks, G. M.; Poulin, P.; Wallace, G. G. Graphene oxide dispersions: tuning rheology to enable fabrication. *Mater. Horiz.* **2014**, 1 (3), 326–331.

(179) Ding, J.; Tracey, P. J.; Li, W.; Peng, G.; Whitten, P. G.; Wallace, G. G. Review on shear thickening fluids and applications. *Textiles and Light Industrial Science and Technology* **2013**, 2 (4), 161–173.

(180) Chen, D. T.; Wen, Q.; Janmey, P. A.; Crocker, J. C.; Yodh, A. G. Rheology of soft materials. *Annu. Rev. Condens. Matter Phys.* **2010**, 1 (1), 301–322.

(181) Liber, S. R.; Borohovich, S.; Butenko, A. V.; Schofield, A. B.; Sloutskin, E. Dense colloidal fluids form denser amorphous sediments. *Proc. Natl. Acad. Sci. U. S. A.* **2013**, 110 (15), 5769–5773.

(182) Kádár, R.; Spirk, S.; Nypelö, T. Cellulose Nanocrystal Liquid Crystal Phases: Progress and Challenges in Characterization Using Rheology Coupled to Optics, Scattering, and Spectroscopy. *ACS Nano* **2021**, 15 (5), 7931–7945.

(183) Buffa, J. M.; Casado, U.; Mucci, V.; Aranguren, M. I. Cellulose nanocrystals in aqueous suspensions: rheology of lyotropic chiral liquid crystals. *Cellulose* **2019**, 26 (4), 2317–2332.

(184) Kiss, G.; Porter, R. S. Rheology of concentrated solutions of poly (γ-benzyl-glutamate). *J. Polym. Sci., Part B: Polym. Phys.* **1996**, 34 (14), 2271–2289.

(185) Araki, K.; Kitano, T.; Hausnerova, B. Rheological properties of carbon fiber and carbon black filled liquid crystalline polymer melts. *Appl. Rheol.* **2001**, 11 (4), 188–196.

(186) Echeverria, C.; Almeida, P. L.; Aguilar Gutierrez, O. F.; Rey, A. D.; Godinho, M. H. Two negative minima of the first normal stress difference in a cellulose-based cholesteric liquid crystal: Helix uncoiling. *J. Polym. Sci., Part B: Polym. Phys.* **2017**, 55 (10), 821–830.

(187) Huang, C.-M.; Magda, J.; Larson, R. The effect of temperature and concentration on N 1 and tumbling in a liquid crystal polymer. *J. Rheol.* **1999**, 43 (1), 31–50.

(188) Song, H.; Zhang, J.; Niu, Y.; Wang, Z. Phase transition and rheological behaviors of concentrated cellulose/ionic liquid solutions. *J. Phys. Chem. B* **2010**, 114 (18), 6006–6013.

(189) Lu, T.; Pan, H.; Ma, J.; Li, Y.; Bokhari, S. W.; Jiang, X.; Zhu, S.; Zhang, D. Cellulose nanocrystals/polyacrylamide composites of high sensitivity and cycling performance to gauge humidity. *ACS appl. mater. interface* **2017**, 9 (21), 18231–18237.

(190) Giese, M.; Blusch, L. K.; Khan, M. K.; Hamad, W. Y.; MacLachlan, M. J. Responsive mesoporous photonic cellulose films by supramolecular cotemplating. *Angew. Chem.* **2014**, 126 (34), 9026–9030.

(191) Hou, Y.; Guan, Q.-F.; Xia, J.; Ling, Z.-C.; He, Z.; Han, Z.-M.; Yang, H.-B.; Gu, P.; Zhu, Y.; Yu, S.-H.; et al. Strengthening and toughening hierarchical nanocellulose via humidity-mediated interface. *ACS Nano* **2021**, 15 (1), 1310–1320.

(192) Feng, K.; Dong, C.; Gao, Y.; Jin, Z. A green and iridescent composite of cellulose nanocrystals with wide solvent resistance and strong mechanical properties. *ACS Sustain. Chem. Eng.* **2021**, 9 (19), 6764–6775.

(193) Guo, F.; Kim, F.; Han, T. H.; Shenoy, V. B.; Huang, J.; Hurt, R. H. Hydration-responsive folding and unfolding in graphene oxide liquid crystal phases. *ACS Nano* **2011**, 5 (10), 8019–8025.

(194) Wani, O. M.; Verpaalen, R.; Zeng, H.; Priimagi, A.; Schenning, A. P. An Artificial Nocturnal Flower via Humidity-Gated Photo-actuation in Liquid Crystal Networks. *Adv. Mater.* **2019**, 31 (2), 1805985.

(195) He, Y.-D.; Zhang, Z.-L.; Xue, J.; Wang, X.-H.; Song, F.; Wang, X.-L.; Zhu, L.-L.; Wang, Y.-Z. Biomimetic optical cellulose nanocrystal films with controllable iridescent color and environmental stimuli-responsive chromism. *ACS appl. mater. interface* **2018**, 10 (6), 5805–5811.

(196) Zhao, G.; Zhang, Y.; Zhai, S.; Sugiyama, J.; Pan, M.; Shi, J.; Lu, H. Dual response of photonic films with chiral nematic cellulose nanocrystals: Humidity and formaldehyde. *ACS appl. mater. interface* **2020**, 12 (15), 17833–17844.

(197) Park, H.-S.; Kang, S.-W.; Tortora, L.; Kumar, S.; Lavrentovich, O. D. Condensation of self-assembled lyotropic chromonic liquid crystal sunset yellow in aqueous solutions crowded with polyethylene glycol and doped with salt. *Langmuir* **2011**, 27 (7), 4164–4175. Vasilevskaya, V.; Khokhlov, A.; Matsuzawa, Y.; Yoshikawa, K. Collapse of single DNA molecule in poly (ethylene glycol) solutions. *J. chem. phys.* **1995**, 102 (16), 6595–6602.

(198) Moud, A. A.; Kamkar, M.; Sanati-Nezhad, A.; Hejazi, S. H.; Sundararaj, U. Viscoelastic properties of poly (vinyl alcohol) hydrogels with cellulose nanocrystals fabricated through sodium chloride addition: Rheological evidence of double network formation. *Colloids Surf., A* **2021**, 609, 125577.

(199) Wan, H.; Li, X.; Zhang, L.; Li, X.; Liu, P.; Jiang, Z.; Yu, Z.-Z. Rapidly responsive and flexible chiral nematic cellulose nanocrystal composites as multifunctional rewritable photonic papers with eco-friendly inks. *ACS appl. mater. interface* **2018**, 10 (6), 5918–5925.

(200) Zhang, Y. P.; Chodavarapu, V. P.; Kirk, A. G.; Andrews, M. P. Nanocrystalline cellulose for covert optical encryption. *J. Nanophotonics* **2012**, 6 (1), 063516.

(201) Xu, M.; Li, W.; Ma, C.; Yu, H.; Wu, Y.; Wang, Y.; Chen, Z.; Li, J.; Liu, S. Multifunctional chiral nematic cellulose nanocrystals/glycerol structural colored nanocomposites for intelligent responsive films, photonic inks and iridescent coatings. *J. Mater. Chem. C* **2018**, 6 (20), 5391–5400.

(202) Happel, J.; Brenner, H. *Low reynolds number hydrodynamics*; Prentice-Hall, Inc.: Englewood Cliff, NJ, 1965; p 331.

(203) Lançon, P.; Batrouni, G.; Lobry, L.; Ostrowsky, N. Drift without flux: Brownian walker with a space-dependent diffusion coefficient. *EPL (europhysics Lett.* **2001**, 54 (1), 28. Lançon, P.; Batrouni, G.; Lobry, L.; Ostrowsky, N. Brownian walker in a confined geometry leading to a space-dependent diffusion coefficient. *Phys. Stat. Mech. it Appl.* **2002**, 304 (1–2), 65–76.

(204) Lin, B.; Yu, J.; Rice, S. A. Direct measurements of constrained Brownian motion of an isolated sphere between two walls. *Phys. Rev. E* **2000**, 62 (3), 3909. Russel, W. B.; Russel, W.; Saville, D. A.; Schowalter, W. R. *Colloidal dispersions*; Cambridge University Press, 1991.

(205) Squires, T. M.; Brenner, M. P. Like-charge attraction and hydrodynamic interaction. *Phys. rev. lett.* **2000**, 85 (23), 4976.

(206) Chen, H.-Q.; Wang, X.-Y.; Bisoyi, H. K.; Chen, L.-J.; Li, Q. Liquid crystals in curved confined geometries: Microfluidics bring new capabilities for photonic applications and beyond. *Langmuir* **2021**, 37 (13), 3789–3807.

(207) Sheikhi, A.; Hayashi, J.; Eichenbaum, J.; Gutin, M.; Kuntjoro, N.; Khorsandi, D.; Khademhosseini, A. Recent advances in nano-engineering cellulose for cargo delivery. *J. Controlled Release* **2019**, 294, 53–76. John, W. S.; Fritz, W.; Lu, Z.; Yang, D.-K. Bragg reflection from cholesteric liquid crystals. *Phys. Rev. E* **1995**, 51 (2), 1191.

(208) Urbanski, M.; Reyes, C. G.; Noh, J.; Sharma, A.; Geng, Y.; Jampani, V. S. R.; Lagerwall, J. P. Liquid crystals in micron-scale droplets, shells and fibers. *J. Phys.: Condens. Matter* **2017**, 29 (13), 133003.

(209) Ji, Q.; Lefort, R.; Busselez, R.; Morineau, D. Structure and dynamics of a Gay–Berne liquid crystal confined in cylindrical nanopores. *J. chem. phys.* **2009**, 130 (23), 234501.

(210) Vigneron, J. P.; Pasteels, J. M.; Windsor, D. M.; Vértesy, Z.; Rassart, M.; Seldrum, T.; Dumont, J.; Deparis, O.; Lousse, V.; Biro, L. P. Switchable reflector in the Panamanian tortoise beetle Charidotella egregia (Chrysomelidae: Cassidinae). *Phys. Rev. E* **2007**, 76 (3), 031907.

(211) Guo, M.; Li, Y.; Yan, X.; Song, J.; Liu, D.; Li, Q.; Su, F.; Shi, X. Sustainable iridescence of cast and shear coatings of cellulose nanocrystals. *Carbohydr. Polym.* **2021**, 273, 118628.

(212) Feng, K.; Gao, X.; Gu, Z.; Jin, Z. Improving homogeneity of iridescent cellulose nanocrystal films by surfactant-assisted spreading self-assembly. *ACS Sustain. Chem. Eng.* **2019**, 7 (23), 19062–19071.

(213) Giese, M.; De Witt, J. C.; Shopsowitz, K. E.; Manning, A. P.; Dong, R. Y.; Michal, C. A.; Hamad, W. Y.; MacLachlan, M. J. Thermal switching of the reflection in chiral nematic mesoporous organosilica films infiltrated with liquid crystals. *ACS appl. mater. interface* **2013**, 5 (15), 6854–6859.

(214) Yi, J.; Xu, Q.; Zhang, X.; Zhang, H. Temperature-induced chiral nematic phase changes of suspensions of poly (N, N-dimethylaminoethyl methacrylate)-grafted cellulose nanocrystals. *Cellulose* **2009**, 16 (6), 989–997.

(215) Parton, T. G.; van de Kerkhof, G. T.; Narkevicius, A.; Haataja, J. S.; Parker, R. M.; Frka-Petesic, B.; Vignolini, S. Chiral self-assembly of cellulose nanocrystals is driven by crystallite bundles. *Nat. Commun.* **2021**, 13, 2657.

(216) Arcolezi, G.; Luders, D.; Sampaio, A.; Simões, M.; Braga, W.; Santos, O.; Palangana, A.; Kimura, N. Computational method to determine the pitch length in cholesteric liquid crystals. *J. Mol. Liq.* **2020**, 298, 111752.

(217) Sui, Y.; Li, X.; Chang, W.; Wan, H.; Li, W.; Yang, F.; Yu, Z.-Z. Multi-responsive nanocomposite membranes of cellulose nanocrystals and poly (N-isopropyl acrylamide) with tunable chiral nematic structures. *Carbohydr. Polym.* **2020**, 232, 115778.

(218) Pan, H.; Ma, J.; Tao, J.; Zhu, S. Hierarchical architecture for flexible energy storage. *Nanoscale* **2017**, 9 (20), 6686–6694.

(219) Walters, C. M.; Matharu, G. K.; Hamad, W. Y.; Lizundia, E.; MacLachlan, M. J. Chiral nematic cellulose nanocrystal/germania and carbon/germania composite aerogels as supercapacitor materials. *Chem. Mater.* **2021**, 33 (13), 5197–5209.

(220) Lizundia, E.; Nguyen, T.-D.; Vilas, J. L.; Hamad, W. Y.; MacLachlan, M. J. Chiroptical, morphological and conducting properties of chiral nematic mesoporous cellulose/polypyrrole composite films. *J. Mater. Chem. A* **2017**, 5 (36), 19184–19194.

(221) Zhang, H.; Li, S.; Qu, A.; Hao, C.; Sun, M.; Xu, L.; Xu, C.; Kuang, H. Engineering of chiral nanomaterials for biomimetic catalysis. *Chem. Sci.* **2020**, 11 (48), 12937–12954.

(222) Prince, E.; Wang, Y.; Smalyukh, I. I.; Kumacheva, E. Cylindrical confinement of nanocolloidal cholesteric liquid crystal. *J. Phys. Chem. B* **2021**, 125 (29), 8243–8250.

(223) Nguyen, T. D.; Li, J.; Lizundia, E.; Niederberger, M.; Hamad, W. Y.; MacLachlan, M. J. Black titania with nanoscale helicity. *Adv. Funct. Mater.* **2019**, 29 (40), 1904639.

(224) Yang, N.; Pattisson, S.; Douthwaite, M.; Zeng, G.; Zhang, H.; Ma, J.; Hutchings, G. J. Influence of stabilizers on the performance of Au/TiO2 catalysts for CO oxidation. *ACS Catal.* **2021**, 11 (18), 11607–11615.

(225) Shopsowitz, K. E.; Hamad, W. Y.; MacLachlan, M. J. Chiral nematic mesoporous carbon derived from nanocrystalline cellulose. *Angew. Chem.Int. Ed.* **2011**, 50 (46), 10991–10995.

(226) Xu, Y.-T.; Dai, Y.; Nguyen, T.-D.; Hamad, W. Y.; MacLachlan, M. J. Aerogel materials with periodic structures imprinted with cellulose nanocrystals. *Nanoscale* **2018**, 10 (8), 3805–3812.

(227) Agumba, J. O.; Adem, J. A.; Barasa, G. O.; Ochung, A. A. The Role of Acid Concentration on Band Gap Shrinkage in Cellulose Nanocrystals Fabricated from Water Hyacinth. *Journal of Material Sciences & Manufacturing Research* **2022**, 3, 1–3.

(228) Kim, K.; Kim, P. J.; Chowdhury, R. A.; Kantharaj, R.; Candadai, A.; Marconnet, A.; Pol, V. G.; Youngblood, J. P. Structural orientation effect of cellulose nanocrystals (CNC) films on electrochemical kinetics and stability in lithium-ion batteries. *Chem. eng. j.* **2021**, 417, 128128.

(229) Wegst, U. G.; Bai, H.; Saiz, E.; Tomsia, A. P.; Ritchie, R. O. Bioinspired structural materials. *Nat. Mater.* **2015**, 14 (1), 23–36.

(230) Kim, S.; Laschi, C.; Trimmer, B. Soft robotics: a new perspective in robot evolution. *Trends Biotechnol.* **2013**, 31, 287–294.

(231) Maeda, S.; Hara, Y.; Sakai, T.; Yoshida, R.; Hashimoto, S. Self-walking gel. *Adv. Mater.* **2007**, 19 (21), 3480–3484.

(232) Liu, K.; Yao, X.; Jiang, L. Recent developments in bio-inspired special wettability. *Chem. Soc. Rev.* **2010**, 39 (8), 3240–3255.

(233) Sun, W. Cellulose reflects left and right. *Nat. Nanotechnol.* **2017**, 1–1.

(234) Harkness, B. R.; Gray, D. G. Left-and right-handed chiral nematic mesophase of (trityl)(alkyl) cellulose derivatives. *Can. J. Chem.* **1990**, 68 (7), 1135–1139.

(235) Santos, M. V.; Tercjak, A.; Gutierrez, J.; Barud, H. S.; Napoli, M.; Nalin, M.; Ribeiro, S. J. Optical sensor platform based on cellulose nanocrystals (CNC)−4′-(hexyloxy)-4-biphenylcarbonitrile (HOBC) bi-phase nematic liquid crystal composite films. *Carbohydr. Polym.* **2017**, 168, 346–355.

(236) Tercjak, A.; Gutierrez, J.; Ocando, C.; Peponi, L.; Mondragon, I. Thermoresponsive inorganic/organic hybrids based on conductive TiO2 nanoparticles embedded in poly (styrene-b-ethylene oxide) block copolymer dispersed liquid crystals. *Acta mater.* **2009**, 57 (15), 4624–4631.

(237) Gan, L.; Feng, N.; Liu, S.; Zheng, S.; Li, Z.; Huang, J. Assembly-induced emission of cellulose nanocrystals for hiding information. *Part. Part. Syst. Charact.* **2019**, 36 (3), 1800412.

(238) Kuo, H.; Chuang, M.; Lin, C. Design correlations for the optical performance of the particle-diffusing bottom diffusers in the LCD backlight unit. *powder Technol.* **2009**, 192 (1), 116–121. Mingyan, L.; Daming, W.; Yajun, Z.; Jian, Z. Optimization and design of LCD diffuser plate with micro-semisphere structure. *Procedia Eng.* **2011**, 16, 306–311.

(239) Chen, C. Y.; Lee, W. K.; Chen, Y. J.; Lu, C. Y.; Lin, H. Y.; Wu, C. C. Enhancing optical out-coupling of organic light-emitting devices with nanostructured composite electrodes consisting of indium tin oxide nanomesh and conducting polymer. *Adv. Mater.* **2015**, 27 (33), 4883–4888.

(240) Fang, Z.; Zhu, H.; Yuan, Y.; Ha, D.; Zhu, S.; Preston, C.; Chen, Q.; Li, Y.; Han, X.; Lee, S.; et al. Novel nanostructured paper with ultrahigh transparency and ultrahigh haze for solar cells. *Nano Lett.* **2014**, 14 (2), 765–773.

(241) Bin, W.; Qing-Kang, W. High sensitivity transmission-type SPR sensor by using Metallic−Dielectric mixed gratings. *Chin. Phys. Lett.* **2008**, 25 (5), 1668.

(242) Liu, Q.; Kuzyk, A.; Endo, M.; Smalyukh, I. I. Colloidal plasmonic DNA-origami with photo-switchable chirality in liquid crystals. *Optics lett.* **2019**, 44 (11), 2831–2834.

(243) Abbasi Moud, A.; Piette, J.; Danesh, M.; Georgiou, G. C.; Hatzikiriakos, S. G. Apparent slip in colloidal suspensions. *J. Rheol.* **2022**, 66 (1), 79–90. Abbasi Moud, A.; Poisson, J.; Hudson, Z. M.; Hatzikiriakos, S. G. Yield stress and wall slip of kaolinite networks. *Phys. Fluid* **2021**, 33 (5), 053105. Danesh, M.; Moud, A. A.; Mauran, D.; Hojabr, S.; Berry, R.; Pawlik, M.; Hatzikiriakos, S. G. The yielding of attractive gels of nanocrystal cellulose (CNC). *J. Rheol.* **2021**, 65 (5), 855–869.